UNIVERSITÀ DEGLI STUDI DI ROMA

"SAPIENZA"

SAPIENZA
UNIVERSITÀ DI ROMA

PHD SCHOOL IN
IMMUNOLOGICAL, HAEMATOLOGICAL AND RHEUMATOLOGICAL SCIENCES
AND
INNOVATION IN IMMUNO-MEDIATED AND HEMATOLOGICAL DISORDERS
XXXII CYCLE

Innovative 3D model for the establishment of primary paediatric brain tumour cultures: new platform for the preclinical study of immunotherapeutic approaches

Coordinator:
Prof.ssa Angela Santoni

Supervisor:
Dr.ssa Del Bufalo Francesca

Candidate:
Belardinilli Tamascia

Anno Accademico: 2019-2020

ABSTRACT

Gliomas, encompassing Low Grade (LGGs) and High Grade (HGGs) diseases are, overall, the most common solid tumors of the pediatric population. Children affected by LGGs that cannot be cured often struggle to obtain a complete remission of the disease, suffering from significant long-term sequelae. HGGs are instead associated with very grim outcomes and no innovative treatment so far has been able to change this poor prognosis. New treatment approaches, such as immunotherapy, are therefore needed for these patients. Gliomas, as all solid tumors, are characterized by a high structural complexity and a strongly immunosuppressive microenvironment, both responsible for the frequent failure of immunotherapeutic approaches. Such complexity is difficult to reproduce with common bidimensional (2D) systems, making the conventional tumor models unable to predict the real efficacy of these treatments. In order to overcome such hurdles and obtain more reliable tumor models, we developed an innovative fibrin-based hydrogel 3D model and tested it as platform to establish primary cultures of pediatric LGGs and HGGs. In particular, LGGs are otherwise extremely difficult to maintain in culture owing to the well-known activation of senescence pathways. To date, 37 samples of LGG were cultured in both 2D and 3D platforms, showing that the 3D-culture enables the stabilization of LGG. Cell lines identity was confirmed by short tandem repeats (STRs) and the immunohistochemical characterization (structure, H&E, Ki67, tumor and differentiation markers) in 3D cultures revealed phenotype and cellular organization closer to those observed in the onset sample, as compared to 2D. The 3D-cultured tumor cells showed a significantly ($p = 0{,}008$) lower senescence rate than 2D. Furthermore, also 6 samples of HGG have been

cultured and established as well. We therefore evaluated the antitumor activity of an innovative immunotherapeutic approach based on the use of γδ-T cells. These cells display properties of both the innate and the adaptive compartment, have a powerful cytotoxic activity, are able to recognize antigens independently from the HLA and display a negligible alloreactivity, resulting extremely attractive for clinical translation in particular for the establishment of an allogeneic "third-party T-cell bank" for ready for use off-the-shelf adoptive T-cell product. The clinical exploitation is limited, however, by the low percentage of circulating γδ-T cells and the lack, to date, of effective culture systems to expand them. We have developed a protocol to expand a clinically relevant number of polyclonal memory γδ-T cells. Artificial antigen presenting cells (aAPC) expressing CD86/4-1BBL/CD40L and cytomegalovirus-pp65 antigen were used to induce γδ-T cell expansion and activation. For increase the safety of our approach aAPCs has been further stable gene-modified with a suicide gene, inducible caspase 9, and then single cell cloned. The γδ-T cells expanded and expressed markers of activation and memory, maintaining a polyclonal phenotype (with a predominantly Vδ1 well known memory infiltrating population), negligible alloreactivity and potent antitumor capacity versus a broad range of malignancies. Lastly, we characterized the antitumor activity of expanded γδ-T cells, as well as of more conventional approaches (such as radiotherapy and chemotherapy), in 2D and in 3D-cultured tumors, showing that the first are significantly more sensitive to treatment. Expanded γδ-T cells showed a relevant antitumor activity in both 2D and 3D, the latter requiring longer cultures to obtain an antitumor control. These data suggest a more realistic estimation of the efficacy of such treatment by the 3D-platform, confirming it as a better model for biological and therapeutic studies.

TABLE OF CONTEST

List of abbreviations

LGG: Low Grade Glioma;

HGG: High grade Glioma;

IDH: Isocitrate dehydrogenase;

TPCV: Thioguanine, Procarbazine, Lomustine, and Vincristine;

NK: Natural Killer;

TCR: T-Cell Receptor;

MHC: Major Histocompatibility Complex;

ADCC: AntibodyDependent Cellular Cytotoxicity;

HSCT: Hematopoietic stem cell transplantation;

HLA: Human Leucocyte Antigen;

PB: Peripheral Blood;

aAPC: Artificial Antigen-Presenting Cell;

CMV: Cytomegalovirus;

PBS: Phosphate-Buffer Saline;

FBS: Fetal Bovine Serum;

GFP: Green Fluorescence Protein;

FFLuc: FireFly-Luciferase;

BSA: Bovine Serum Albumine,

iC9: Inducible Caspase 9;

PBMC: Peripheral blood mononuclear cells;

BC: Buffi Coats;

HD: Healthy donors;

ECM: Extra-Cellular Matrix.

Legend of figures

Legend of table

Table 1: Comparison of 2D and 3D cell culture methods.

Table 2: Details of the histology of the LGGs and HGGs samples cultured in 2D and 3D platforms.

Table 3: Results of STR evaluation of the sample of one representative patient and of the relative 2D and 3D cultures.

INTRODUCTION

1.1 Brain Tumors

Central nervous system tumors are the most common solid tumors of childhood, and gliomas comprise the majority of central nervous system tumors. The term glioma describes central nervous system tumors that arise from glial cells, in either the brain or the spine (Figure 1). As with most central nervous system tumors, gliomas were first described and classified by Harvey Cushing and Percival Bailey in the first few decades of the 20th century. The clinical presentation of childhood gliomas is extremely heterogeneous and is highly dependent on the localization of the lesion. This heterogeneous group of tumors has been classified and graded by the World Health Organization based on their histological and molecular features (Figure 2).

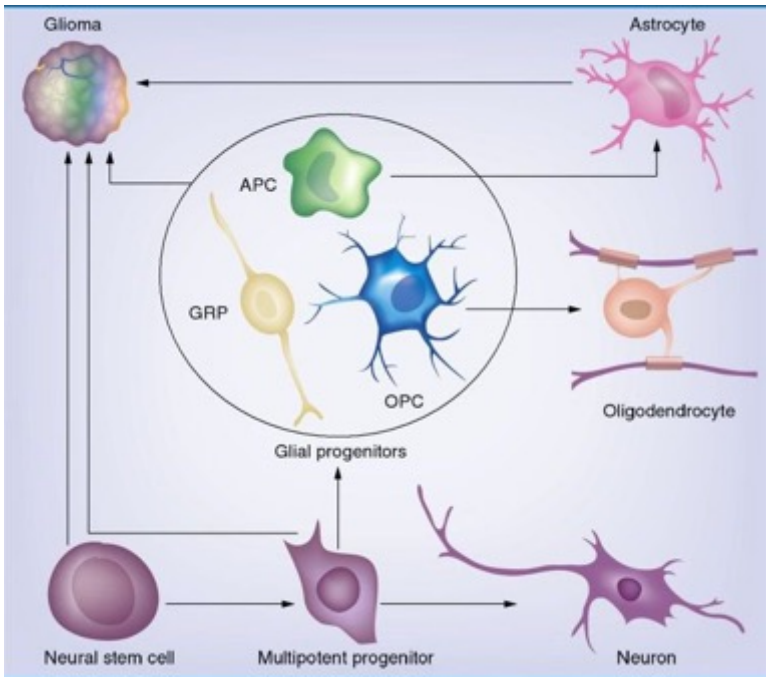

Figure 1: Schematic representation of normal glial cells from which gliomas derived. Modified from The Cellular Origin for Malignant Glioma and Prospects for Clinical Advancements. Expert Rev Mol Diagn. 2012;12(4):383-394.

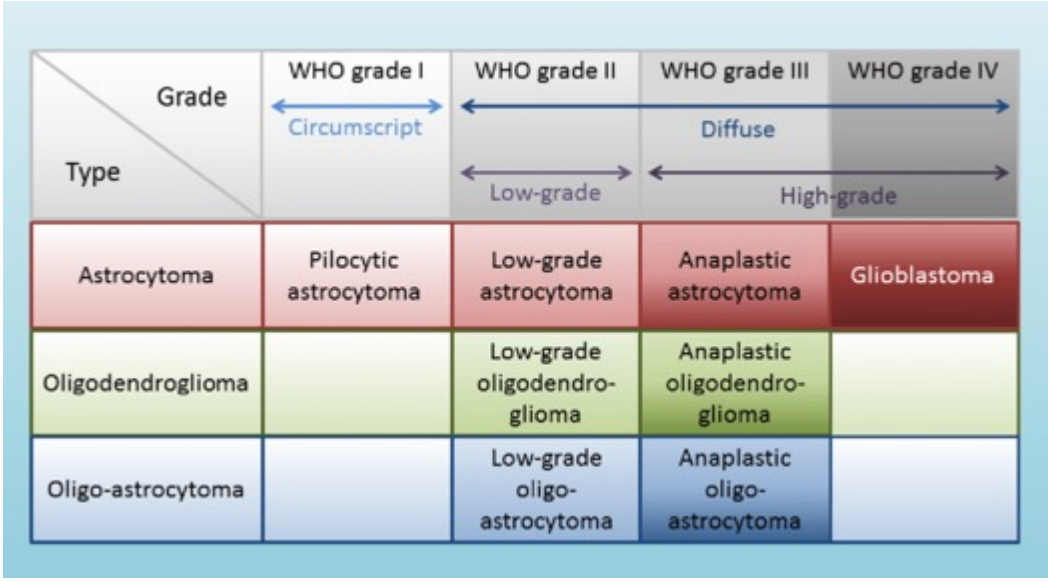

Figure 2: Classification of gliomas in types and WHO grades. Modified from Taal W.r & Bromberg JEC & Bent M. (2015). Chemotherapy in glioma. CNS oncology. 4. 1-14. DOI:10.2217/cns.15.2.

As shown in figure 2, it includes astrocytomas, which are graded low grade gliomas (**LGGs**) (grades I and II astrocytomas) and high-grade gliomas (**HGGs**), such as anaplastic astrocytomas (grade III) and glioblastomas (grade IV) [1-2]. Today, gliomas of all grades account for up to 50% of pediatric central nervous system tumors [3]. Pediatric LGG constitute almost 40% of pediatric brain tumors and are composed mainly of WHO grade I pilocytic astrocytoma, which accounts for 20% of brain tumors in patients under the age of 20 years, alone. The morphological features of pilocytic astrocytomas are distinctive and characterized by extensive vascular proliferation, biphasic architecture, Rosenthal fibers, eosinophilic granular bodies, and occasionally, regions of limited calcification. Gangliogliomas are another LGG (grade I) of mixed neuronal-glial subtype, also characterized by granular bodies and regions of calcification, and also exhibit binucleated neurons and cystic degeneration. Other LGG of childhood include subependymal giant-cell astrocytoma (WHO grade I), fibrillary/diffuse astrocytoma (grade II), pilomyxoid astrocytoma (grade II), pleomorphic xanthoastrocytoma (grade II), oligodendrogliomas (grade II),

and oligoastrocytomas (grade II). In recent years, advances in genomics and molecular diagnostics have revolutionized the classification of pediatric gliomas. Indeed, one effect of this has been to shift the focus away solely from a purely morphological classification to a more molecular based stratification, which not only provides a more robust risk stratification, but also offers the possibility of new and novel targets for therapy [2]. Low-grade gliomas typically have a protracted clinical course while high-grade tumors usually have a more acute presentation with rapid progression of symptoms. The number of genetic alterations commonly found in pediatric LGG is fairly limited and in the case of pilocytic astrocytomas is predominantly a 1-pathway disease. Indeed, the majority of pilocytic astrocytomas harbor lesions in the MAPK pathway [4]. In addition, mutations in the tumor suppressor gene TP53 [5], metabolic genes, IDH1 and IDH2 [6] and point mutations or gene fusion in in $BRAF^{V600E}$ [7] are also common in adult LGG but exceedingly rare in childhood LGG [8-9]. However other mutations have been described in gliomas and a representative schema of these are shown in figure 3.

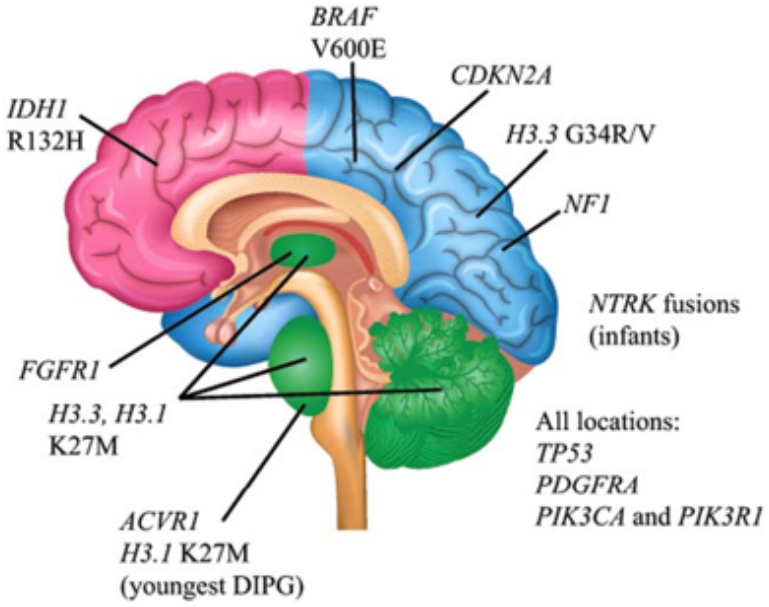

Figure 3.: Spatiotemporal association of mutations in pediatric high-grade glioma. Modified from Pediatric gliomas as neurodevelopmental disorders Suzanne J. Baker, David W.Ellison, David H. Gutmann.06 december 2015.Glia.

1.1. Treatment of Low-Grade Gliomas

Patients with low-grade gliomas are primarily treated by surgical resection of the tumor. Patients with complete tumor resection typically do not require any adjuvant therapy. However, complete tumor resection can be challenging or impossible, and is highly dependent on the location of the tumor. Consequently, surgical management of low-grade gliomas patients is aimed at maximal safe surgical resection [10-11]. In the case of recurrence, additional therapeutic approaches, such as radiation therapy and chemotherapy, can be utilized. Three adjuvant therapies are currently available for progressive and unresectable low-grade gliomas; external beam irradiation, conventional chemotherapy and targeted therapies. There are several first line approaches for conventional chemotherapy for LGGs including carboplatin and vincristine, TPCV (thioguanine, procarbazine, lomustine, and vincristine) and weekly vinblastine monotherapy [12-13]. All these approaches are well tolerated have been shown to stabilize disease progression in up to 50% of patients. However, in many instances, treatment needs to be repeated 2 or 3 times prior to complete disease stabilization. External beam irradiation in low-grade gliomas, although effective is reserved for older children and for cases where chemotherapy options have been exhausted. The majority of children with low-grade gliomas survive long-term and as such, the side effects of radiation therapy particularly cognitive side effects, vasculopathies and hormonal imbalances outweigh its benefits. It would be important to identify new therapeutic approaches, such as immunotherapy or target therapy, especially for those LGGs that require adjuvant therapies, and also because, as mentioned above, often the therapies can have severe side effects.

1.2. Immunotherapy: a new frontier for cancer treatment

The principal biological role of the immune system is to maintain the integrity of "self". This integrity is maintained principally by eliminating and destroying diseased and infected cells, while ensuring that healthy cells and tissues are not targeted. Several evidences exist to document that the immune system plays a role in controlling the growth of tumour cells. Hence, in the past few years, the rapidly advancing field of cancer immunology has produced several new methods of treating cancer, called immunotherapies, which increase the strength of immune responses against tumours. Immunotherapies either stimulate the activities of specific components of the immune system or counteract signals produced by cancer cells that suppress immune responses. Such immunotherapeutic strategies include a plethora of vaccine-based methods to trigger anti-tumor cellular and humoral immunity, antibody strategies to mediate complement and NK-dependent anti-tumor cytolytic activity, block inhibitory receptors, or modulate the tumor microenvironment, oncolytic virus and adoptive cell transfer strategies [14]. A number of immunotherapy drugs are already used in cancer treatment and even more await the results of the latest clinical tests.

1.3. Universal adoptive T cell therapy approach: γδ-T cells

Although in the last decades remarkable progress has been made in the outcome of patients affected by oncological malignancies, many of them still suffer from either relevant toxicities or have relapsed/refractory

disease. Innovative and less toxic treatment strategies are therefore urgently needed [15-16]. Emerging evidences highlight the possibility to strengthen the ability of the immune system to identify, seek out and destroy malignant cells. Due to their well-known intrinsic immunosurveillance properties, components of the innate immune system might represent promising platforms for innovative immunotherapy approaches. γδ T cells represent one of the major components of the innate immune system with distinct T cell receptor (TCR) γ and δ chains on their surface, which account for 0.5–5% of all T-lymphocytes. This small subset of cells was first described in 1987, after the accidental discovery of a third chain of the TCR (γ chain) in 1984 [17-18]. In contrast, most of the T cells in the healthy human instead are T cells (65–70%) with a TCR composed of two glycoprotein chains called α and β TCR chains. Although, γδ T cells are much less frequent than αβ T cells; they are at their highest abundance in the gut mucosa, within a population of lymphocytes known as intraepithelial lymphocytes [18-19]. Their features include non-MHC restricted antigen recognition and an abundant cytokine secretion capacity. These attractive features have raised expectations for their application in cancer adoptive immunotherapy [20]. Similar to αβ T cells, their polyclonality has been demonstrated crucial for exerting a potent cytotoxic activity against bacteria, viruses and distinct types of cancer and they have high capacity to physiologically infiltrate the microenvironment of solid tumours [21]. Therefore, focusing also on their function as professional antigen presenting cells (APC), several studies underline the role of γδ-T cells in boosting the response of the immune system [22]. Then, based on their biological function, γδ T cells can also be divided into two distinct subsets: effector γδ T cells and regulatory γδ T cells. When γδ T cells are activated by a stimulus, the cells, that play an antitumor role by secreting cytokines, act through antibody dependent cellular cytotoxicity (ADCC) effects, as well as other processes, and

therefore are referred to as effector γδ T cells. These cells migrate to the local tumor environment and have the capacity to lyse cancer cells through the perforin-granzyme pathway [23]. For example, in renal cancer, γδ T cells have shown to display a selective lytic potential towards autologous primary renal cancer cells, but not against normal renal cells, an effect mediated mainly depending on the TCR and the NKG2D receptor [24]. Several clinical trials emphasized the therapeutic potential [25-26]. For example, long-term remission of leukaemia amongst allogeneic haematopoietic stem cell transplantation (HSCT) recipients transplanted from a human leucocyte antigen (HLA)-disparate donor correlates with increased engraftment frequency of donor-derived γδ-T cells [27]. A potent ex-vivo anti-tumour activity of isolated γδ-T cells has also been clearly shown in patients after HLA-haploidentical αβ-T-cell depleted HSCT [28]. In this heterogeneous population, the γδ T cells expressing a TCR containing γ-chain variable region 9 (Vγ9) and δ-chain variable region 2 (Vδ2), known as Vγ9/Vδ2 T cells, showed in numerous pre-clinical and clinical studies a potent anti-tumor activity, inhibit cancer cell proliferation, angiogenesis, lymphangiogenesis, and increase cancer cell apoptosis [29-30]. Vγ9/Vδ2 T cells can recognize phosphorylated antigens that accumulate in cancer cells, interact with the F1-ATPase expressed on the cancer cell surface, and recognize stress-induced molecules, such as the MHC class I chain-related molecules A and B (MICA and MICB), as well as UL16-binding proteins [31]. In contrast, Vδ1 and Vδ3 γδ T cells comprise only a minor subset of this population. In particular, Vδ1 γδ T cells showed activity against glioblastoma and are found in normal human epithelia, dermis, spleen and liver, as well as in the peripheral blood of patients with chronic viral infections and patients with leukemia correlating with their complete response[32-33-34].This population has also been associated with clinical benefits due to its more naïve memory phenotype [35] the reduced

susceptibility to activation-induced cell death [36] and its natural residency in tissues. Little is known on Vδ1negVδ2negVδ3neg population, and it has been suggested that this subset has a role in both anti-viral and anti-tumor immunity [37-38]. Moreover, as mentioned above γδ-T cells have the peculiar ability of recognizing antigens in an MHC independent manner [39] and are capable to activate macrophages and dendritic cells [40-41]. Their negligible alloreactivity makes them optimal candidates for the generation of a third-party, off-the-shelf and ready-to-use, T-cell bank. Although these characteristics render γδ-T cells extremely attractive as platform for immunotherapies, their low frequency in peripheral blood (PB) poses a relevant limitation for their clinical exploitation [35]. Expansion protocols conventionally used to propagate αβ-T cells fail at initiating and sustaining γδ-T-cell growth [42-43]. To date, large-scale ex vivo γδ-T cell expansion is limited to the $V\delta2^+$ population, particularly Vγ9Vδ2, which can be expanded through the administration of Zoledronic Acid [44-45]. The adoptive transfer of these cells showed clinical responses in the treatment of both solid and hematological malignancies [45-46]. Other studies demonstrated the expansion of γδ-T cells using either plant-derived T-cell mitogens [47-48] or artificial antigen-presenting cells (aAPC) engineered to express costimulatory ligands [49]. However, all these protocols were incapable of inducing the expansion of sufficient numbers of Vδ1 tissue-infiltrating/virus-specific γδ-T cells; moreover, a safety mechanism to eliminate aAPCs in vivo was not included.

1.4. Cell culture models

Studies on the mechanisms underlying the formation, function and pathology of tissues and organs are manageable largely due to the use of cell culture systems and animal models [50].Nowadays, experiments can be conducted using primary cells isolated directly from the donors' biopsies or using established cultures deposited in cell banks [51]. Characteristic features of primary cells are difficulties with isolation and short life span. On the other hand, they closely mimic the in vivo genetic features of tumors and thus make it possible to perform some functional experiments. Cell cultures make it possible to understand cell biology, tissue morphology, mechanisms of diseases, drug action, protein production and the development of tissue engineering [52]. They are often used in the preclinical research of many drugs, in cancer research, and in studies on gene function [51]. The choice of the most appropriate cell culture methods in the area of cancer research may al-low us to better understand tumor biology, and hence to optimize radio- and chemotherapy, or even to find new treatment strategies [53]. The most commonly used type of cell culture is the 2D model, but recently the 3D culture method has been gaining in popularity because has proved to be particularly promising for studying cellular behavior respecting the microenvironment and cellular organization (figure 4) [54]. Depending on the type of culture chosen, cell behavior in fact differs in many aspects [52].

A

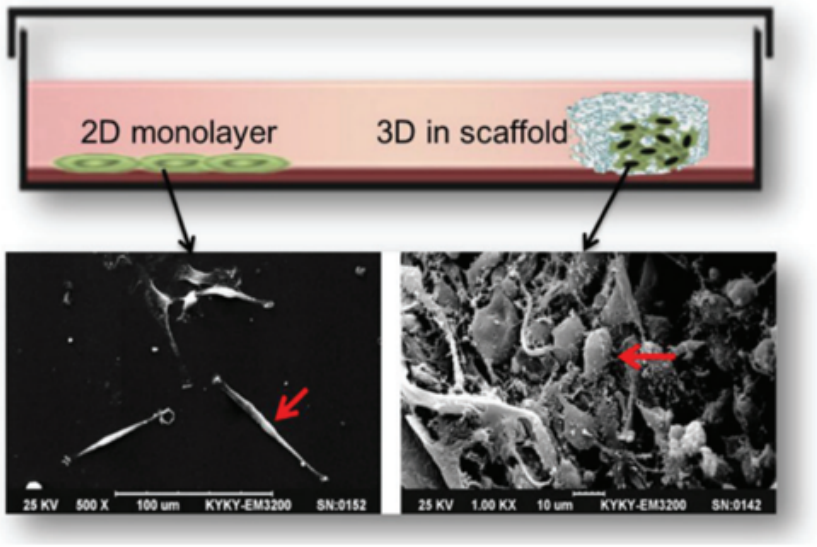

Figure 4: Different cell organization in 2D and 3D cultures. Comparison of tumor cells morphology between 2D and 3D scaffold culture. U87 cells in 2D (left) and 3D scaffold (right) in a scanning electron microscope image. **Modified from: Three-dimensional cell culture: A powerful tool in tumor research and drug discovery (Review). Donglai LV et al. Oncology letters July 27, 2017.**

1.5. 2D Culture

In adherent 2D cultures, cells grow as a single layer attached to a plastic or glass surface [55]. 2D crops have the advantage of being easy to make and cheap. 2D cultures also have numerous disadvantages. Since the cells are distributed on a cellular monolayer, they cannot imitate the structure and organization assumed by the cells in their natural environment. In this culture method, interactions with the microenvironment and cell-cell extracellular cells are limited compared to those in vivo. These interactions are responsible for cell differentiation, proliferation, vitality, gene and protein expression, stimulus reactivity, drug metabolism and other cellular functions [54-56-57]. Furthermore, the cell morphology and the proliferative rate are also altered. The different organization and morphology of cells in 2D cultures can influence their function [58-59]. Furthermore, cells growing in plates forming a cellular monolayer lose their polarity [60], this modifies the response of cells to different phenomena, such as apoptosis [61-62]. Another notable difference that cells in 2D cultures present with respect to the in vivo situation is the availability of oxygen, nutrients, metabolites and signal molecules. In fact, in vivo, the availability of these factors is extremely variable due to the architecture of the cells within the tumor mass [54], while in 2D cultures all cells are equivalent and have easy access to nutrients and oxygen. Furthermore, several studies underline how the 2D grown is able to modify the gene profile of the cells []. Moreover, in 2D cultures not only the maintenance of cellular architecture is lacking but above all the microenvironment, fundamental for tumor development. Because of these disadvantages, it was necessary to find alternative models, able to imitate the cellular organization and the tumor microenvironment, such as the use of 3D culture systems (Table 1).

	2D Model	3D Model
In vivo imitation	Do not mimic the natural structure of the tissue or tumor mass	Microenvironment exhibits unique biochemical and morphological features representative of the in vivo state
Cell interactions	Deprived of cell-cell and cell-extracellular environment interactions	Proper interactions of cell-cell and cell-extracellular environment
Characteristics of cells	Changed morphology and way of divisions; loss of diverse phenotype and polarity	Preserved morphology and way of divisions, diverse phenotype and polarity
Access to essential compounds	Unlimited access to oxygen, nutrients, metabolites and signalling molecules (in contrast to in vivo)	Variable access to oxygen, nutrients, metabolites and signaling molecules (same as in vivo)
Molecular mechanisms	Changes in gene expression, mRNA splicing, topology and biochemistry of cells	Expression of genes, splicing, topology and biochemistry of cells as in vivo
Cost of maintaining a culture	Cheap, commercially available tests and the media	More expensive, more time-consuming, fewer commercially available tests

Table 1: Comparison of 2D and 3D cell culture methods. Modified from: 2D and 3D cell cultures a comparison of different types of cancer cell cultures M. Kapałczyńska et al.

1.6. 3D Culture

Tumor cells grown in 3D platforms form multicellular tumor spheroids or organoids. Organoids are aggregates of tumor cells grown in suspension or incorporated in gel using 3D culture methods. One of the first three-dimensional crops was made in a soft agar solution and was made from Hamburg and Salmon in the 1970s [65]. Since then, new methods and materials have been used. There are different methods used to create 3D models, each has advantages and disadvantages, that can be divided into: cultures in suspension on non-adherent plates, cultures in concentrated medium or in gelatinous substance and cultures on a scaffold. 3D cultures can be created with donor cells, these are grown in three-dimensional

structures, mimicking the architecture of the derivation tissue more accurately than is possible in 2D models [66]. This characteristic of 3D models is the result of cell-cell and environment interactions, created to imitate the structure of the tissue. Furthermore, cells can receive stimuli from local invasion, as happens in vivo [67-68]. In 3D cultures, the morphology and polarity of cells are maintained contrary to what happens in 2D [69-70]. In 3D cultures there is a difference in the proliferation dependent on the localization of the cells in the organoid, this is greater in the peripheral part of the 3D structures [71-72]. Another important feature of 3D cultures are that they exhibit gene expression, signaling and metabolism similar to the in vivo situation [73-74]. All these features make it possible for the 3D model to be used as a specific platform to study cancer cells in a context that recapitulates invasion and metastatic processes as well as escape mechanisms.

1.7.3D model as a platform for preclinical studies

Tumorigenesis is a complex and largely unknown process, dependent on multiple mechanisms, including the 3D architectural structure and the interaction between malignant and stromal cells in the tumor microenvironment [75-76]. Conventional 2D cell culture systems in which the specific tissue architecture, cell-cell and cell-matrix interactions and signaling between cellular residence within distinct niches are absent can't summarize this interactivity [77]. In vitro altered biology of tumor cells and support of stroma impact on the pharmacological responses observed in vitro, reducing the predictive power of preclinical tests [78]. This limitation is particularly evident when complex therapies such as the use of immunotherapeutic approaches are tested. Cells cultured in 3D scaffolds

better recapitulate the in vivo architecture of tumors and display similar gene expression [79]. By increasing the correspondence between ex vivo cell culture and in vivo tumor growth, 3D cultures can improve the relevance of ex vivo studies and increase the predictive power of in vitro drug testing [80]. In our study, we use pegylated fibrin-based hydrogels, which solve various limitations that other models present, in fact they are quick to realize, it is possible to vary the concentration of fibrinogen by adapting the system to different cultures and varying the mechanical properties of gel of fibrin. Also, they are transparent and can be followed over time. It is a highly biocompatible and versatile system for a series of in vitro studies ranging from immunohistochemistry to live analysis. Moreover, thanks to its plasticity it can also be easily degraded allowing the whole recovery of the entire tumor heterogeneity without cell damage or alteration of surface molecules. All these features make this model optimal for realizing primary cultures and studying characteristics of the tumor and its biology.

AIMS OF THE PRESENT STUDY

- Establishment of primary pediatric brain tumor cultures

- Development of a new platform for the pre-clinical evaluation of immunotherapeutic approaches.

- method to efficiently expand polyclonally-activated γδ-T cells using aAPCs expressing costimulatory molecules, the CMV-pp65 antigen and an inducible safety switch in order to generate an off-the-shelf, stand-alone treatment or as bridging therapy to more targeted immunotherapeutic approaches.

MATERIALS AND METHODS

2.1. Patients and generation of 2D and 3D primary Low-Grade Glioma lines.

We collected data from 40 consecutive pediatric patients diagnosed with Low Grade Glioma (LGG) in our Institution, from 1st January 2016 to 31st July 2019. Diagnosis was based on clinical, radiological criteria and immunopathological evaluation. Samples were mechanically processed, washed twice with phosphate-buffered saline (PBS) (1200rpm for 10 minutes) and re-suspended in a GBM complete media [DMEM (Thermo Scientific-Rome, Italy) supplemented with 10% Fetal Bovine Serum (Thermo Scientific), 1% L-glutamine (EuroClone, Milan - Italy), 1% penicillin/streptomycin (EuroClone), 1% sodium pyruvate 100mM (EuroClone), 1% MEM non-essential amino acids (EuroClone) and 2% of sodium bicarbonate solution (Sigma Aldrich, St Louis, MO - USA)] in order to obtain a cell suspension. Cells were then seeded in 24 well plates to create 2D and 3D primary cultures. All samples were obtained after the approval of the institutional review board of Bambino Gesù Children's Hospital.

2.2. Cell lines

All tumour cell lines were purchased from ATCC or DSMZ. K562 were cultured in RPMI1640 (Thermo Scientific) supplemented with 10% FBS and 2 mM GlutaMax (Thermo Scientific, Pittsburgh, PA, USA). The glioblastoma cell lines U87 and U373 were cultured in DMEM supplemented with 10% FBS and 2 mM GlutaMax. The 293T cell lines were

cultured in IMDM (Thermo Scientific), supplemented with 10% FBS and 2 mM GlutaMax. Cells were maintained in a humidified atmosphere containing 5% CO_2 at 37°C. All cell lines were routinely tested for mycoplasma infection and authenticated by short tandem repeat analysis (Eurofins Genomic, Ebersberg, Germany).

2.3. Vector design and transient transfection.

Retroviral and lentiviral vectors were generated to stably transduce K562, an immortalized leukaemia cell line. The retroviral vector was designed to encode the cDNA of CD86, 41BBL and the inducible caspase-9 (iC9) suicide gene using SFG retroviral backbone [81], while the lentiviral vectors encode the cDNA for CMV-pp65 with or without the costimulatory molecule CD40L. An additional retroviral vector encoding eGFP-Firefly-Luciferase (eGFP-FFLuc) was used to label tumour cells for *in-vitro* studies, as previously described [82-83-84].

2.4. Preparation of PEG-fibrin hydrogel components and cell retrieval

Fibrin/PEG-based hydrogels were prepared as previously described [88]. Human fibrinogen (Sigma Aldrich,) was solubilized in PBS at a concentration of 80 mg/mL. After 2h of incubation at 37°C, the solution was filtered using a 0.20 mm SteriFlipfilter (EMD Millipore, Billerica, MA - USA). Succinimidyl-glutarate-modified bifunctional polyethylene glycol [3.4 kDa SG-PEG-SG (PEG); NOF America Corporation, White Plains, NY - USA] was dissolved in PBS at 8 mg/mL and filtered with a 0.2 mm syringe. Fibrinogen and PEG solutions were combined in a 1:1 volume ratio, mixed

thoroughly, and incubated at 37°C. PEGylated fibrinogen was then mixed at a 1:1 volume ratio with the cell solutions (1,2e5 cells/mL of U373 eGFP-FFLuc and U87 eGFP-FFLuc; or processed cell suspensions of samples from pediatric LGG). Human thrombin (Sigma Aldrich) was diluted to 25 U/mL in sterile 40 mM $CaCl_2$ (CalBiochem, La Jolla, CA - USA) and incubated at 37°C before use. To retrieve cells from the hydrogel, a fibrinolytic solution was prepared by dissolving 75 mg/mL (fibrin degradation units) of nattokinase (NSK-SD; Japan BioScience Laboratory Co., Ltd) in PBS containing 1 mM EDTA. The hydrogels were subsequently dissolved by adding 1 ml of the fibrinolytic solution and incubating at 37°C for 20 minutes [85].

2.5. Immunofluorescence staining

Primary cell lines were grown in complete media for at least 5 days in 24 multi-well glass plates. When 2D and 3D primary cell lines reach 80% of confluence, medium was removed, and the cells were washed with PBS (300uL/well 2 times for 1 minute). Cells were fixed with Paraformaldehyde 4% in PBS (CYTOFIX, BD Biosciences, San Jose, CA, USA) (300uL/wells 10 minutes at room temperature (RT)) and then washed with PBS (300uL/wells 2 times from 5 minutes). Then, cells were washed with IFF buffer (PBS 1X + 5% FBS + 2% Bovine Serum Albumine SIGMA-aldrich, St.Louis,USA) (300uL/well for 5 minutes) and permeabilized with 0,5% Triton for 10 minutes at RT and finally washed 2 times with PBS and 2 times with IFF for 5 minutes. After a fixation and permeabilization, the cultures were blocked with 10% normal goat serum (SIGMA-aldrich, St.Louis,USA), in PBS 300 ul/well for 1h at RT while shaking. Following the unspecific site block, cells were incubated with primary antibodies [polyclonal rabbit anti-human glial

fibrillary acid protein (DAKO, L'Aquila, Italy); polyclonal rabbit anti-human XOlig-2 (Millipore); monoclonal mouse anti-human Synaptophysin (Dako); polyclonal chicken anti-human Ki-67 (Immunological sciences, Gainesville Florida, USA); polyclonal rabbit anti-human anti-p16 (Immunological sciences); monoclonal mouse anti-human p53 (Immunological sciences) with at least 200 ul/well, overnight for 2D cultures and for two days in the dark at 4°C for 3D cultures . Cells were then washed twice with PBS (300ul/well) and with IFF buffer (300ul/well) and incubated with the secondary antibodies resuspended in IFF buffer, 200ul/well [goat anti-rabbit Alexa Fluor 555F(ab*)IgG(H+L) (Thermo Fisher Scientific, Vanallen Way, Carlsbad, USA; 1:1000); goat anti-mouse Alexa Fluor 488 (Thermo Fisher Scientific; 1:1000); donkey anti-chicken Alexa Fluor 488 IgY (IgG)(H+L) (Immunological sciences; 1:1000) for 2h in the dark for 2D cultures and 2 days in the dark for 3D cultures while shaking. After incubation cells were washed with PBS (300ul/well) for 5 minutes and incubated with Hoechst dye (Hoechst 33342 trihydrocloride trihydrate, Invitrogen, Monza, Italy) for nuclear staining for 30 minutes in the dark at 4°C. Finally, cells were washed twice with PBS followed by 50% glycerol in PBS (300ul/ well) and stored at 4°C. Fluorescence signals were detected using confocal microscopy (Leica DMi8, Leica, Rome, Italy). All acquisitions were performed in non-saturated single z-confocal planes and images were captured from randomly selected fields of view.

2.6. Immunohistochemistry staining

Hydrogels were collected and fixed in 4% formaldehyde for 24h at RT for paraffin embedding and haematoxylin/eosin or immunohistochemistry staining. Human GFAP (Glial Fibrillary Acid Protein) and Olig-2 immunodetection was performed by incubating paraffin-embedded hydrogel sections with a primary polyclonal rabbit anti-GFAP antibody (Dako, 1:50) or a polyclonal rabbit anti-Olig-2 antibody (Millipore, 1:200). For detection Dako LSAB + System-HRP (Dako) was used. Stained sections were scored in a blinded manner by a pathologist F. Diomedi Camassei.

2.7. Artificial Antigen Presenting Cell (aAPC) generation

aAPCs were generated using the K562 cell line. The cells were first transduced with lentiviral vectors encoding either human pp65/eGFP or CD40L/pp65 [82]. Then cells were additionally transduced with a retrovirus vector encoding human CD86, 4-1BBL and iC9. After transduction, single cell clones were generated.

2.8. Phenotypic analysis

Expression of cell surface molecules was determined by flow-cytometry using standard methodology. Anti-human monoclonal antibodies were purchased from BD Biosciences, Miltenyi and eBiosciences. Samples were analysed with a BD LSR-Fortessa X-20 and analysed by FACS-Diva

software (BD Biosciences). For each sample, a minimum of 20,000 events were acquired.

2.9. Cytokine profile

Supernatants collected after 24h of co-culture were analysed using immunoassays incorporating magnetic microsphere technology (Millipore), according to the manufacturer's instructions, as previously described [86].

2.10. Ex-vivo isolation and expansion of polyclonal αβ- and γδ-T cells

Peripheral blood mononuclear cells (PBMC) were isolated from buffy coats (BC) obtained from healthy donors (HD) at Bambino Gesù Children's Hospital after written informed consent was signed, in accordance with the rules set by the Institutional Review Board (N°969/2015 prot. N° 669LB), using Lymphoprep™ density gradient medium (Eurobio, Courtaboeuf, France). αβ-T lymphocytes were activated with immobilized OKT3 (1 μg/ml, e-Bioscience, San Diego, CA, USA) and anti-CD28 (1 μg/ml, BD Biosciences, Franklin Lakes, NJ, USA) monoclonal antibodies, while γδ-T cells were isolated using the γδ isolation kit (Miltenyi, Bergisch-Gladbach, Germany) and stimulated weekly with irradiated aAPCs. T cells were expanded in medium containing 45% RPMI1640 and 45% Click's medium (Sigma-Aldrich), supplemented with 10% FBS and 2 mM GlutaMAX in a humidified atmosphere in the presence of IL2 ($2.1x10^4$ U/ml, R&D, Minneapolis, MN, USA) for αβ-T lymphocytes; for γδ-T cells IL2 ($2.1x10^4$ U/ml), IL12 ($4.5x10^5$ U/ml, Miltenyi), IL15 ($3x10^6$ U/ml, R&D), and

IL21 ($2x10^4$ U/ml) (Miltenyi) were used for the first stimulation, while IL2 and IL15 for the following 3-4 weekly stimulations.

2.11. Co-culture assay

For co-culture experiments, αβ- or γδ-T cells were plated at the indicated Effector:Target (E:T) ratios with or without supplementation of IL2/IL15 in the presence of eGFP-FFLuc tumor cells. Bioluminescence signals of 2D and 3D cultures were evaluated overtime adding 20 ug/ml of D-Luciferin K^+ salt (Perkin Elmer,Waltham,MA, US). At days +6 and +14 of co-culture, cells were collected, and residual tumour evaluated by flow-cytometry [81-87].

2.12. Senescence associated Galactosidase (SA-β-gal) Activity Assay

To assess senescence, we used the Senescence β-Galactosidase Staining Kit (Cell Signaling Technology, Danvers, MA, USA). Primary 2D and 3D cell lines were cultured in 6 well plates until 70% of confluence. Cells were washed twice with 2mL of PBS followed by 1 ml/well of a fixative solution. for 10-15 minutes at RT. Then, the cells were rinsed twice with PBS and successively incubated with 1 ml/well of the β-Galactosidase Staining Solution. Plates were sealed in order to avoid evaporation and incubated at 37°C O/N in a dry incubator. Nucleic staining was performed with DAPI. The analysis was performed by fluorescence microscopy (LEICA DMC4500 LEICA Microsystem, Buccinasco ; ITALY).

2.13. Cell Proliferation and MTT Assay

To evaluate cell proliferation after several treatments, we used CellTiter 96 AQueous one solution Cell Proliferation Assay (MTT Assay) (Promega, Milan, Italy). Immortalized as well as 2D and 3D primary cell lines were cultured for 2 days and 5 days, respectively, in 48 multi-well plates, and then treated with ionizing radiation, administration of vincristine or infection with oncolytic adenovirus. After 7 or 14 days of treatment, the medium was removed from 2D and 3D cultures and the hydrogels dissolved by the fibrinolytic solution. Then 40 ul/well of MTT was added into each well containing the samples in 200ul of PBS. The plate was subsequently incubated at 37°C for 2 hours in a humidified, 5% CO_2 atmosphere. Viability was assessed by measuring the absorbance at 492 nm with a plate reader (SYNERGY H1 microplate reader, BioTeK, Winooski, VT-USA).

2.14. Irradiation of immortalized and primary 2D and 3D cultures

Cells were seeded at a density of $7x10^3$ cells/well in 24 well plates and maintained under appropriate culture conditions. The following day for the 2D model and at day +4 for the 3D model, the cells were irradiated with 80 Gy and 160 Gy using a (RADGIL2, GILARDONI s.p.a ,IRA01A1).The plates were placed in the incubator at 37°C. After 7 days of culture the cell viability was evaluated by MTT assay.

2.15. Treatment of immortalized and primary 2D and 3D cultures with vincristine

Cells were seeded at a density of $7x10^3$ cells/well and maintained under appropriate culture conditions. The following day for the 2D model and at day +4 for the 3D model, the medium was removed, and the cells treated with increasing concentrations of vincristine (SIGMA Aldrich): $1x10^{-4}$ M, $1x10^{-2}$ M, $1x10^{-1}$ M and 0 M in 1mL of complete culture media. The plates were placed in the incubator at 37°C. After 7 days of culture the cell viability was evaluated by MTT assay.

2.16. Statistical Analysis

Unless otherwise noted, data is summarised as average ± standard deviation (SD) from at least three independent experiments. Statistical significance was measured using a paired Student's T test, assuming a two-tailed distribution, one-way and two-way analysis of variance (ANOVA) followed by Tukey's post hoc test. Graph generation and statistical analyses were performed using Prism version 6.0d software (GraphPad, USA).

RESULTS

3.1. Sophisticated qualitative and quantitative monitoring of glioma tumor growth with the 3D hydrogel platform.

U87 and U373 immortalized cell lines were first used to set up the 3D conditions. After genetically modifying the glioma cells with a retroviral vector encoding the Green Fluorescent Protein (GFP) in tandem with the FireFly-Luciferase (FF/Luc) (Figure 5A), they were plated in the pegylated fibrin (PEG-fibrin) hydrogel 3D scaffold, as previously described [88].

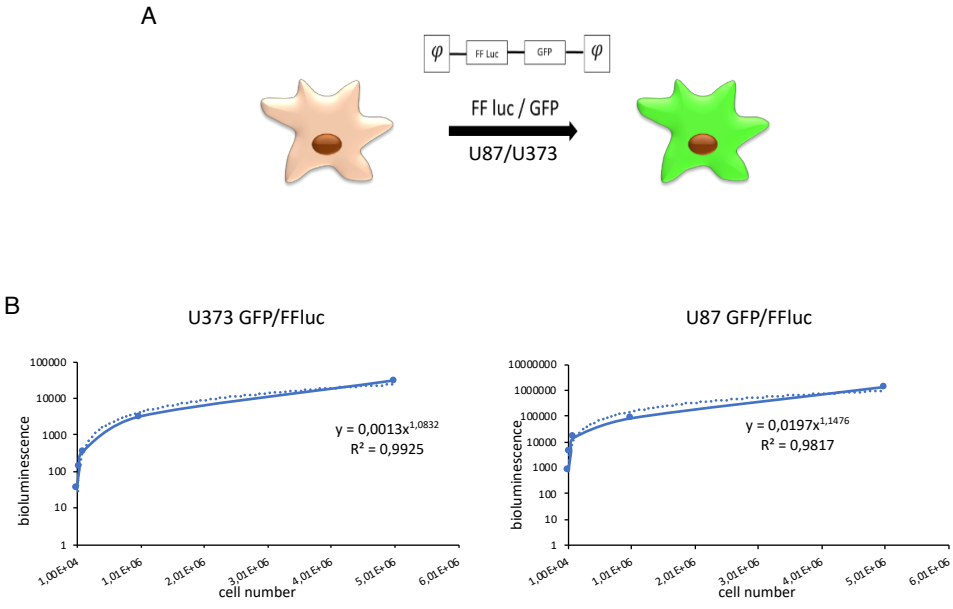

Figure 5: Correlation between bioluminescence signal and number of cells in the Hydrogel. Schematic representation of the retroviral vector encoding GFP and FF/Luc used to transduce tumour cell lines U87/U373 (**A**). Quantitative correlation between the number of GFP/FFluc-U373 (graph on the left) and GFP/FFluc-U87 (on the right) and the bioluminescence signal(**B**)

In order to monitor the cell growth, the bioluminescence signal was acquired and correlated with the number of seeded cells. We were then able to draw a curve correlating reliably the bioluminescence signal and the cell number in the hydrogels. This allowed us to obtain a quantitative measurement of the cellular growth without disrupting the system (figure 5B). Moreover, we recapitulated the 3D architecture and organization of the cells in the hydrogel through a confocal microscopy reconstruction of the GFP^+ tumor cells, performed acquiring images on the x, y and z axes. As shown in figure 6A-B, the U87 cells self-assemble in the tridimensional area, organizing into complex organoid structures.

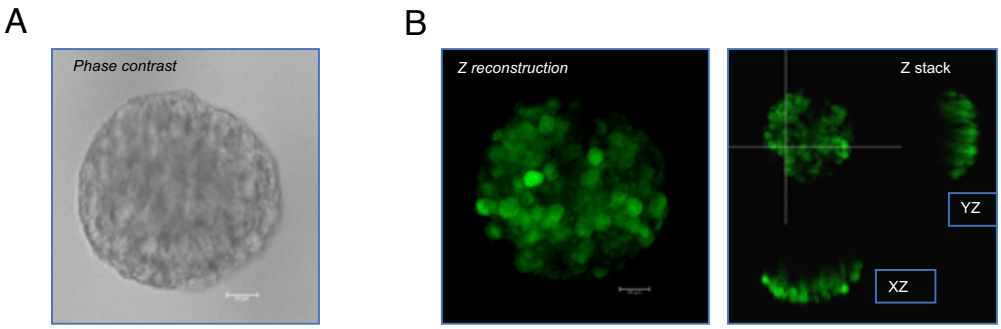

Figure 6: Confocal microscope images of 3D cultures of U87. Image of an organoid in bright field (60x) (**A**). Cell morphology of GFP^+ cells analyzed through confocal microscopy and the reconstruction along three axes x, y and z (60x) (**B**).

3.2. The 3D platform allows the establishment of primary cell lines of LGGs displaying more complex structures and more regular growth rate, as compared to conventional 2D cultures.

After establishing the ability of the PEG-fibrin hydrogel to sustain the growth of glioma cell lines into complex 3D structures, we proceeded into a more complex system by culturing primary cell lines derived from pediatric brain tumors samples. In particular, upon approval from the IRB, brain tumor samples were received by the Neurosurgery and Neuro-oncology Unit of the Ospedale Pediatrico Bambino Gesù (OPBG), on the day of the surgery. Each sample was readily processed and subsequently cultured in both conventional two-dimensional (2D) and three-dimensional (3D) platforms simultaneously, as shown in the cartoon of the figure 7A. All the samples of gliomas, from grade I (WHO) to grade IV (WHO) received was cultured upon receipt. However, we focused particularly on the establishment of cultures of LGGs, considering the well-known early *in vitro* activation of senescence pathways in these tumor cells. This phenomenon leads to a substantial impossibility of maintaining and expanding LGGs cells in culture and therefore to a lack of a reliable *in vitro* cellular model for these tumors. Moreover, in order to avoid the selection of any subpopulation in the culture, we did not include any growth factor or special additive in the culture media. Up to date, 45 LGG samples and 6 HGG samples have been collected and cultured. The histological diagnosis of the tumors are shown in details in Table 2. Table 2 also shows

that the engraftment capacity of the 3D scaffold structure is greater than the same sample grown in 2D, showing how this model is better at maintaining primary cultures of LGG.

Histology	TOT	2D	3D
LGG	**45**		
Astrocytomas	19	11	18
Gangliogliomas	18	5	14
Other histology	8	4	6
HGG	**6**		
Anaplastic astrocytomas	3	1	3
Diffuse intrinsic pontine glioma	2	1	2
Anaplastic ganglioglioma	1	0	1

Table 2: Details of the histology of the LGGs and HGGs samples cultured in 2D and 3D platforms. The overall number of samples cultured after surgery is shown as total; the relative cultures stably established in 2D and 3D are shown in each column, for each histology.

The cultures were then followed overtime and growth monitored by conventional microscopy. As shown in Figure 7B, when cultured in the 3D platform, the cells derived from the tumor samples self-organize into complex 3D structures, with multiple and differentiated compartments, suggesting an interplay between different cell types. On the contrary, 2D cultures display a simple, more homogeneous, monolayer distribution (figure 7B).

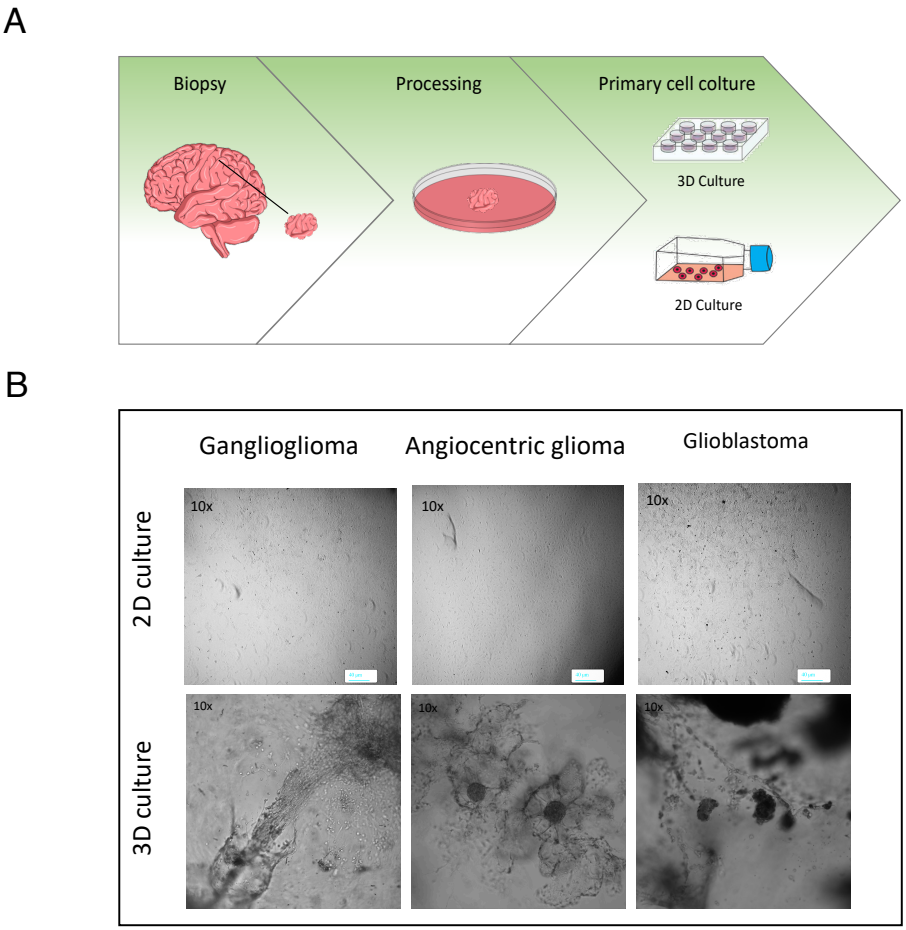

Figure 7: Generation and expansion of primary cultures from pediatric brain tumors. Schematic representation of the processing of brain tumor samples to set up primary 2D and 3D cultures (**A**). BF pictures of 2D (upper panel) and 3D (lower panel) primary cultures of paediatric brain tumours (10X). (**B**).

When the primary cell cultures reached a confluence of 70-80%, either in the 2D or in the 3D conditions, we subcultured the cells for continued growth and to stimulate further proliferation, obtaining secondary cell cultures. The analysis of the secondary cell cultures obtained and maintained overtime in 2D, and 3D is shown in figure 8A. In both the platforms, ganglioglioma and low grade astrocytomas represent the more frequent histology, reflecting the epidemiology of LGGs in the patient population. We did not observe any advantage of establishment and growth for any histology. We further characterized the tumor growth kinetics in the 2 culture conditions by

analyzing the average days of cultures between each passage, focusing on the first 7-8 passages. As shown in the figure 8B, the average culture days of each passage is comparable between the 2 platforms at the first passage and becomes progressively shorter in the 2D cultured tumors, as compared to the 3D, up to step 3-4 where we have a significant difference ($p = 0.0005187$) between the two models, reaching a stability at passage 5-6. reaching a stability at passage 5-6. On the contrary, the average days between passages of the 3D cultured cells maintained longer than the 2D cultured cells and more regular between every passage. The lower rate of growth observed in the 3D tumors is more representative of the real growth kinetic of these tumors, in humans, known to develop over several months or even years. On the other hand, the increasingly rapid growth of the 2D cultures may suggest the selection of transformed cells.

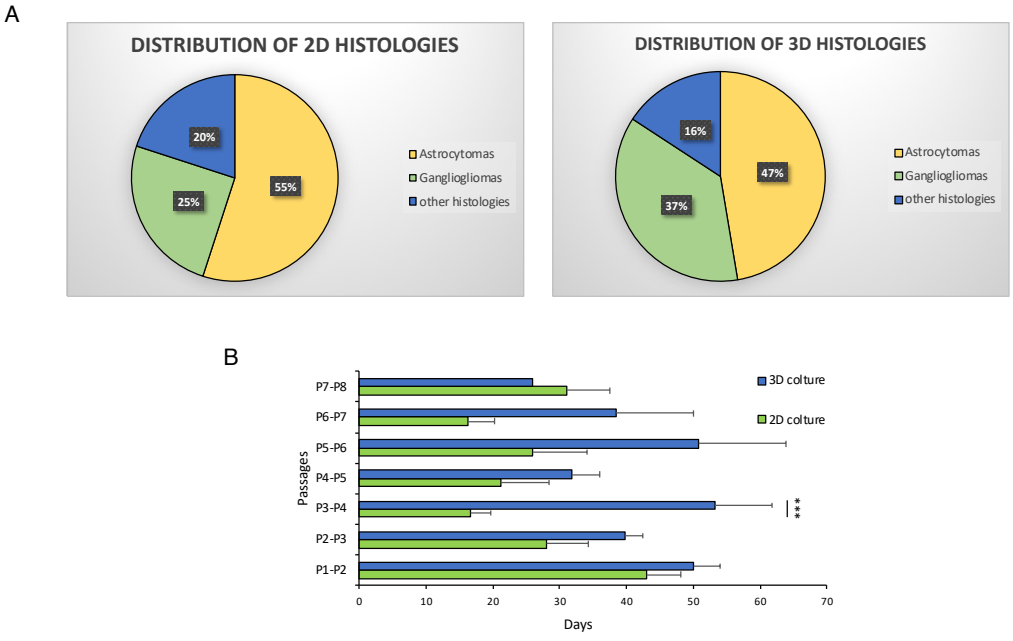

Figure 8: Difference of tumour engraftment rate in 3D and 2D culture. The average duration of each culture passage, expressed in days, in the 2D and 3D model (N=from 30 to 2) (**B**). The pie chart shows the percentage distribution of LGG in 3D and 2D culture (**A**)

3.3. Primary LGG lines show morphology, structural organization and histopathology closely resembling the tumor of origin in the 3D organoids.

After obtaining subcultured LGGs cell lines, we characterized both the 2D cultured and the 3D cultured cells. At first, we authenticated the cells to confirm the origin by performing short tandem repeat (STR) profiling, the recommended method for the purpose of authentication [89]. As shown in table 3, identity between the patient sample and the cultures was confirmed.

Loci	Patient sample	2D	3D
AM	X, X	X, X	X, X
D3S1358	15, 18	15, 18	15, 18
D1S1656	14, 15	14, 15	14, 15
D6S1043	19, 19	19, 19	19, 19
D13S317	11, 13	11, 13	11, 13
Penta E	11, 12	11, 12	11, 12
D18S51	12, 15	12, 15	12, 15
D2S1338	18, 18	18, 18	18, 18
CSF1PO	12, 13	12, 13	12, 13
Penta D	10, 11	10, 11	10, 11

Table 3: Results of STR evaluation of the sample of one representative patient and of the relative 2D and 3D cultures.

Subsequently, we characterized the nature of the subcultured cells, for histopathologic confirmation, by evaluating the organoids morphology and the expression of specific tumor markers. In details, we processed the hydrogels by paraffin embedding and obtained sections that were then stained by either hematoxylin and eosin (H&E), immunofluorescence (IF) or immunohistochemistry (IHC). once stained, the 3D organoids were compared with the tumor sample at onset (representative sample in figure 9A). As shown in the figure 9A, in the 3D organoid the cells acquire a spindle shape and organize in tumor aggregate with a complex organization that closely resembles the tumor of origin. Beside the morphological organization of the tumor, as shown in figure 9A, the 3D organoid displays a positivity at IHC for the glial fibrillary acidic protein (GFAP) and a negativity for Olig-2, corresponding to the IHC signature of the tumor of origin (Figure 9A). These results confirm that not only the 3D culture has grown and organized as the tumor of origin, but also that it maintains its histological characteristics. The 2D cultured cells could not be analyzed for these features, since they lack by definition a structural organization.

Therefore, to further characterize the histopathology of both the 2D and 3D cultured cells, all the primary cultures were analyzed by IF. Figure 9B shows the staining of 2 representative 3D and 2D cultured cell lines derived from 2 distinct LGGs samples. In the 3D culture the cells are morphologically heterogeneous. Two large central cells can be distinguished, showing an elevated expression of GFAP and Synaptophysin; other smaller cells show a weak colocalization of the two markers. Lastly, Olig-2 is expressed homogeneously by all the cells (figure 9B). In the classical two-dimensional culture, the histopathology of the cell line is confirmed as well but the cells appear more homogeneous in size and

for the expression of the 3 markers analyzed. These results suggest that the 3D platform is more suitable than conventional bidimensional systems for growing primary LGG cell lines that better recapitulate the morphology, the organization and the heterogeneity of the tumor of origin.

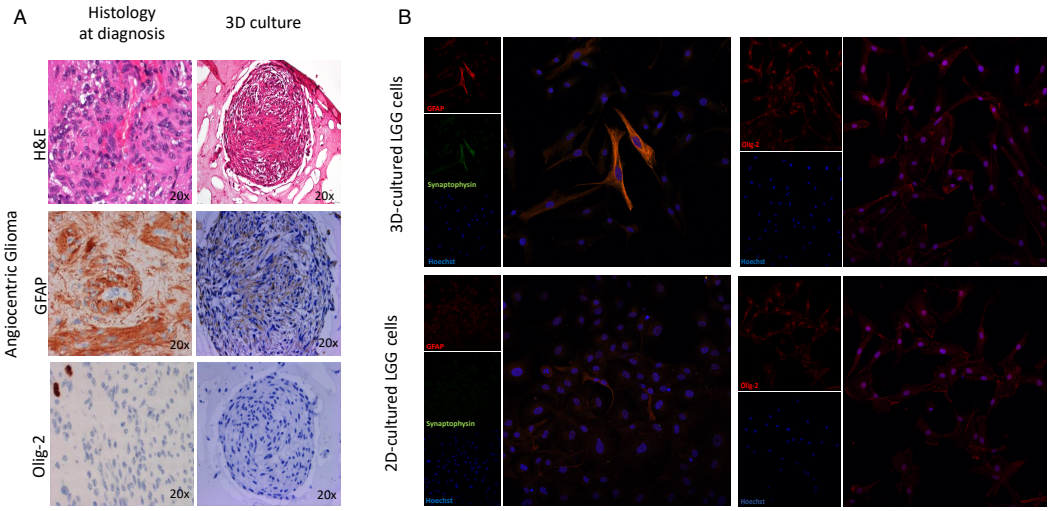

Figure 9: Characterization by IHC and IF of 2D and 3D cultures derived from samples of LGGs. Sections of a sample of angiocentric glioma at diagnosis and a 3D expanded primary culture from the same tumor were compared by H&E and IHC for GFAP and Olig-2 (20X) (**A**). Image acquired by confocal microscopy of 2 primary cultures of LGGs, stained for GFAP (red), synaptophysin (green) and olig-2 (red); nuclei are marked by Hoechst (blue). The upper panel shows a 3D culture, the lower panel a 2D culture (20X) (**B**).

3.4. Differently from the conventional 2D cultures, 3D-cultured LGGs cell lines have a lower rate of activation of senescence.

After establishing the cultures, confirming their authentication and assessing the histopathology and phenotypic closer similarity to the tumor of origin in the 3D-culture, we evaluated whether the same platform could also recapitulate more realistically key biological functions of the cells. In particular, we focused first on the activation of the senescence pathway. In fact, the early activation of this pathway represents a well-known limitation to the possibility of maintaining LGG cells in conventional culture. The establishment of stable cell lines that can be used to evaluate cellular behavior in response to different treatments is therefore difficult to obtain. We observed that the cells grown in 2D cultures exhibited phenotypic changes that resembled those observed in cells undergoing senescence, including a flattened cell morphology with enlarged cell size. In contrast, the cell lines grown in the 3D platform maintained a regular morphology overtime. We next examined the senescence by combining the 2 most established methods: the evaluation of the endogenous SA-β-gal activity (pH 6.0) and the staining for the markers of senescence (p53, p16 and Ki-67). As shown in a representative patient in figure 10A, a stronger SA-β-gal activity was seen in 2D-cultured cells as compared to 3D grown cells.

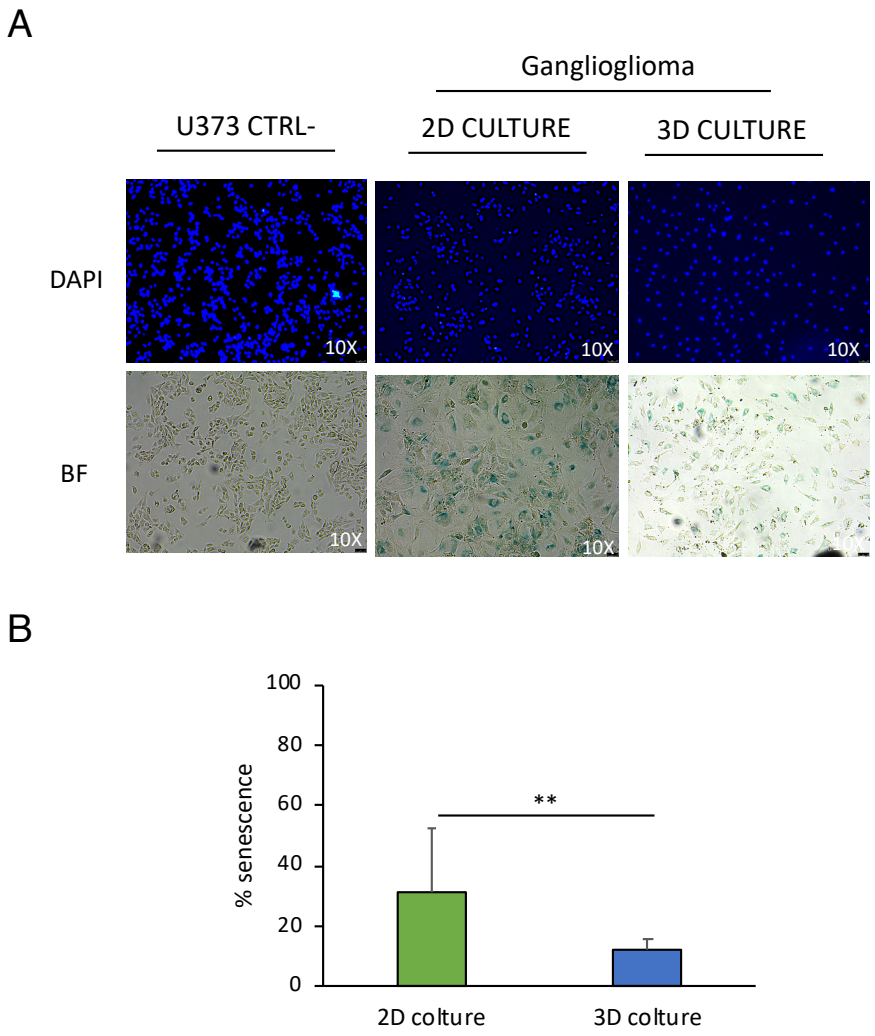

Figure 10: Evaluation of senescence level in 2D and 3D cultured cells. Images acquired by confocal microscopy of the nuclei, stained in blue with Hoechst (on the top), and of the β-Galactosidase staining at ph 6.0 in BF (at the bottom), on U373 (Negative control, CTRL), 2D and 3D primary cultures derived from the same representative patient (**A**). Cumulative analysis of the percentage of senescent cells of primary 2D and 3D cultured cells deriving from LGGs (n=4), data are expressed as average ± SEM. **p<0.01 (**B**).

In order to quantify the activity, the percentage of senescent cells was quantified in 4 patients, cultured in both 2D and 3D conditions, at the same timepoint of culture. As shown in Figure 10B, the percentage of senescent cells in 2D cultures is significantly greater than the 3D cultures ($p = 0.007$). In primary cells, premature senescence involves the overexpression of the tumor suppressors, such as p53 and p16, associated with a low proliferation index, expressed by the low/absent positivity for the nuclear Ki-67.

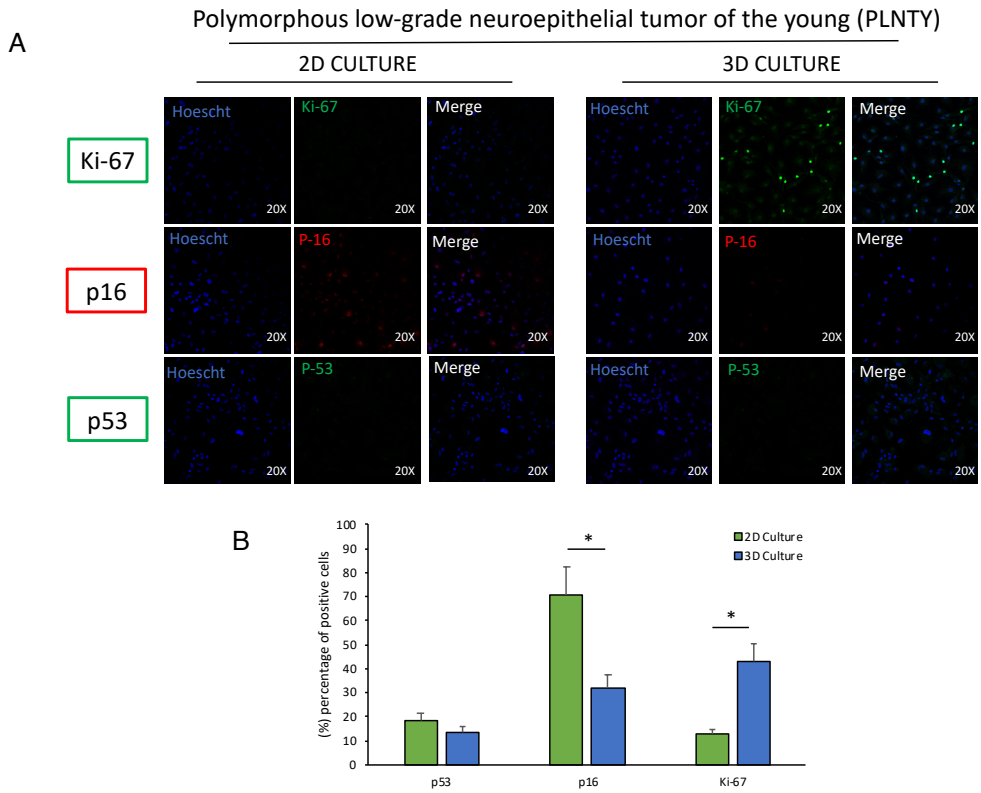

Figure 11: expression of p53, p16 and ki-67 in primary LGG cultures. Two representative 2D and 3D primary cultures derived from the same LGG tumor sample, were stained by IF and acquired through confocal microscopy (20X). The nuclei are stained in blue with Hoechst, the ki-67 in green, p16 in red and p53 in green (**A**). Analysis of the percentage of Ki-67, p16 and p53 positive cells in 3 primary cultures, both 2D and 3D (for each patient, 6 different fields were evaluated); data are expressed as average ± SEM. *p<0.05 (**B**).

We therefore evaluated the expression of these 3 markers by IF on 3 primary LGGs 2D and 3D cultures. In the Figure 11A, the expression of these markers on 2D and 3D primary cultures derived from a Polymorphous low grade neuroepithelial tumor of the young (PLNTY) is shown in detail. In the 2D culture, a greater expression of p16 with a remarkable decrease of the expression of ki-67 is observed, as compared to the 3D culture (figure 11A). The percentage of p16, p53 and Ki-67 positive cells in 3 2D and 3 3D primary cultures of LGGs was then evaluated, as shown in figure 11B. The cell lines cultured in 2D have a significantly higher percentage of p16 positive cells than the 3D-cultured cells ($p = 0{,}025$). At the same time, in the 3D cultures the cells are more actively proliferating, as compared to 2D,

clearly shown by the significantly higher percentage of positive Ki-67 cells (p=0.02) (figure 11B). The positivity of p53 remains comparable in the 2 models. These data clearly show that in the 3D model there is a lower activation of the senescence pathways, allowing the development of primary LGGs cultures.

3.5. The 3D-cultured LGG cell lines display a kinetic of response to conventional treatment that more closely predicts the clinical response than the 2D cell lines

After verifying that the morphologic and biological behaviour, in terms of growth and senescence, of the 3D-cultured LGGs primary cell lines was more realistically representative of the tumor of origin, we wanted to verify whether this could translate into a more realistic prediction of the response to treatments, therefore ultimately offering a more reliable platform for screening the activity of innovative approaches. Therefore, we first compared the response to the two conventional approaches used to treat this kind of tumor: radiotherapy and chemotherapy (vincristine). Several primary LGG 2D-cultured and 3D-cultured cells were treated with increasing doses of ionizing radiation (0 Gy, 80 Gy and 160 Gy) (Figure 12A) or with different concentrations of the chemotherapy agent vincristine (0M, $1X10^{-4}$M, $1X10^{-2}$M, $1X10^{-1}$M) (Figure 12B). Seven days after irradiation or after treatment with vincristine, we evaluated the cell viability through MTT assay. As shown in Figure 12, for both the approaches, the cells in 2D cultures have a greater sensitivity to both the treatments, shown by the reduced vitality as compared to the 3D cultures.

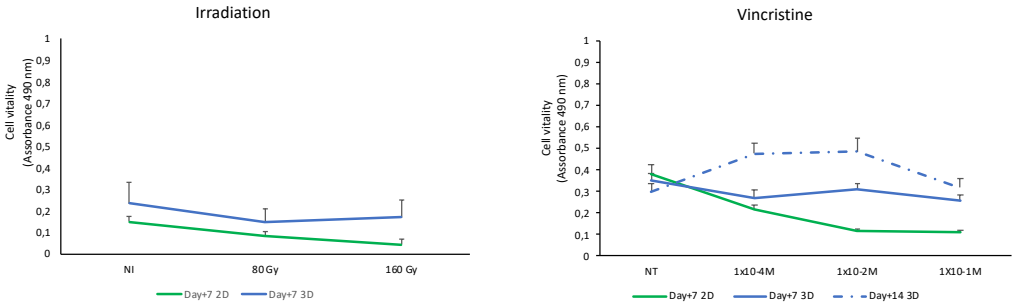

Figure 12: Evaluation of the response of 2D and 3D cultures to conventional treatments. Cell viability of cells in 2D and 3D cultures was tested by MTT assay 7 days after irradiation with 0 Gy, 80 Gy or 160 Gy (**A**) or after the administration of different vincristine doses: 0M, $1X10^{-4}$M, $1X10^{-2}$M, $1X10^{-1}$M (**B**). Data summarized as average ± SEM of 3 2D and 3D cultures. *$p<0.05$.

Differently from the response observed in the 2D cultures, the kinetic of the 3D cell lines is more coherent with that observed in the treatment of pediatric LGG: these tumors are, in fact, sensitive to radiotherapy, although the response is generally slow, and obtain a substantial stabilization of disease with the chemotherapy treatment. These results suggest that the 3D hydrogel provides a better model to predict response to treatment, offering an innovative tool for more detailed therapeutic studies.

3.6. Development and validation of a universal ready-to-use immunotherapeutic approach for the treatment of cancer based on the expanded and activated polyclonal γδ memory T cells.

We therefore aimed at exploiting this well-established platform for studying more advanced immunotherapeutic approaches. At our laboratory, we developed a strong expertise in the use of adoptive therapies, especially for genetically modified T-cells expressing either a transgenic αβ T-cell receptor (TCR) or a chimeric antigen receptor (CAR), to redirect the cytotoxic potential of αβ T cells against tumor cells. Despite the extraordinary efficacy observed in the treatment of Acute Lymphoblastic Leukemia (ALL) with a CAR redirected against the CD19 antigen (PMID: 25317870), similar results have not been yet reached in the treatment of solid tumors where the results are still suboptimal. Innovative approaches are therefore required for these patients. As explained in paragraph "1.3", innate T-cells are a heterogeneous population expressing a TCR composed of γ- and δ-chains and exerting a cytotoxic activity against bacteria, viruses and tumors. These cells have a very good ability to infiltrate into tissues, the peculiar capacity of recognizing antigens in a major histocompatibility complex independent fashion [90] and are capable of producing cytokines, not only directly but also indirectly, by stimulating macrophages and dendritic [40-41]. Their negligible alloreactivity makes them optimal candidates for the generation of a third-party, off the shelf and ready-to-use, T-cell bank. All these characteristics make γδ-T cells extremely attractive as platform for immunotherapies but their low frequency in peripheral blood poses a relevant limitation for their clinical exploitation [35]. *In vitro* expansion is therefore needed. For this reason, we decided to focus our attention on the generation of a protocol to expand polyclonal and activated γδ-T cells for their clinical application.

3.7. Potent *ex vivo* γδ-T-cell expansion is driven by the combination of CD86/41BBL with CD40L and pp65 CMV costimulation.

Polyclonality and activated phenotype of γδ-T cells, together with an efficient expansion, are essential to achieve a functional and effective T-cell product. For this reason and due to the incapacity of these cells to expand with the conventional protocols used to propagate αβ-T cells, we generated aAPCs expressing different costimulatory molecules, including CD86, 41BBL, CD40L and the CMV-pp65 antigen in order to initiate and sustain the γδ-T-cell activation using retroviral and lentiviral vectors (Figure 13A). In a translational perspective, we improved the safety profile by stably transducing aAPCs with the iC9 suicide gene, which is a system already validated in a clinical setting (PMID: 22047558). After generating stable and clonal aAPCs (Figure 13A and B), γδ-T-cells were isolated from PBMCs of HD using the Miltenyi magnetic beads negative selection system. Purity was assessed after selection, showing 96.9%±1.4% γδ-T-cells, 0.3%±0.2% TCR-$\alpha\beta^+$ and 0.9%±0.3% Natural Killer (NK) cells (Figures 14). The isolated cells were then stimulated with irradiated aAPC, either wild type (WT), +/+ (iC9, CD86 and 41BBL), pp65 (+/+ and pp65) or CD40L/pp65 (+/+, pp65 and CD40L); aAPCs were used as feeder cells at a ratio of 1:2 (γδ-T:aAPCs) and cultured with sequential cytokine administrations.

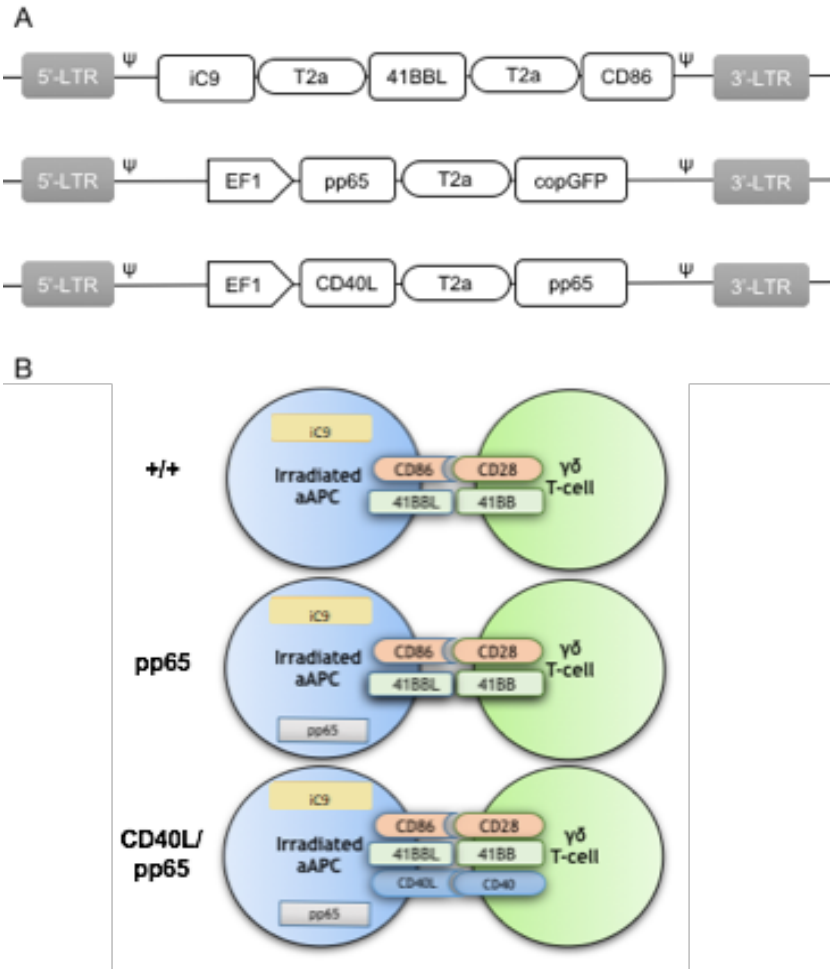

Figure 13: Schematic representation of the viral vectors used in the study. Retroviral and lentiviral vectors used to transduce aAPCs (**A**). The K562 cell line was engineered to express a combination of different costimulatory molecules and the iC9 safety switch and used as aAPCs (**B**).

The most efficient expansion was achieved when γδ-T cells were stimulated with CD40L/pp65_aAPCs (313±70 fold increase at day+28), compared to WT, +/+ and pp65 [16±10 ($p<0.0001$), 25±15 ($p<0.0001$) and 104±50 ($p<0.001$), respectively]. Moreover, only γδ-T cells stimulated with aAPCs including pp65 (CD40L/pp65 and pp65) showed a sustained proliferation rate until day+28, while those stimulated with +/+ and WT_aAPCs reached a plateau at day+21, followed by a decrease until day+28 (figure 15). In order to assess the safety of the proposed expansion protocol, we first evaluated the presence of remaining aAPCs in the γδ-T cell preparations. As shown in figure 16A-B, in none of the infused products, aAPCs were detected by neither cytofluorimetric nor more sensitive molecular (short tandem repeat) analysis.

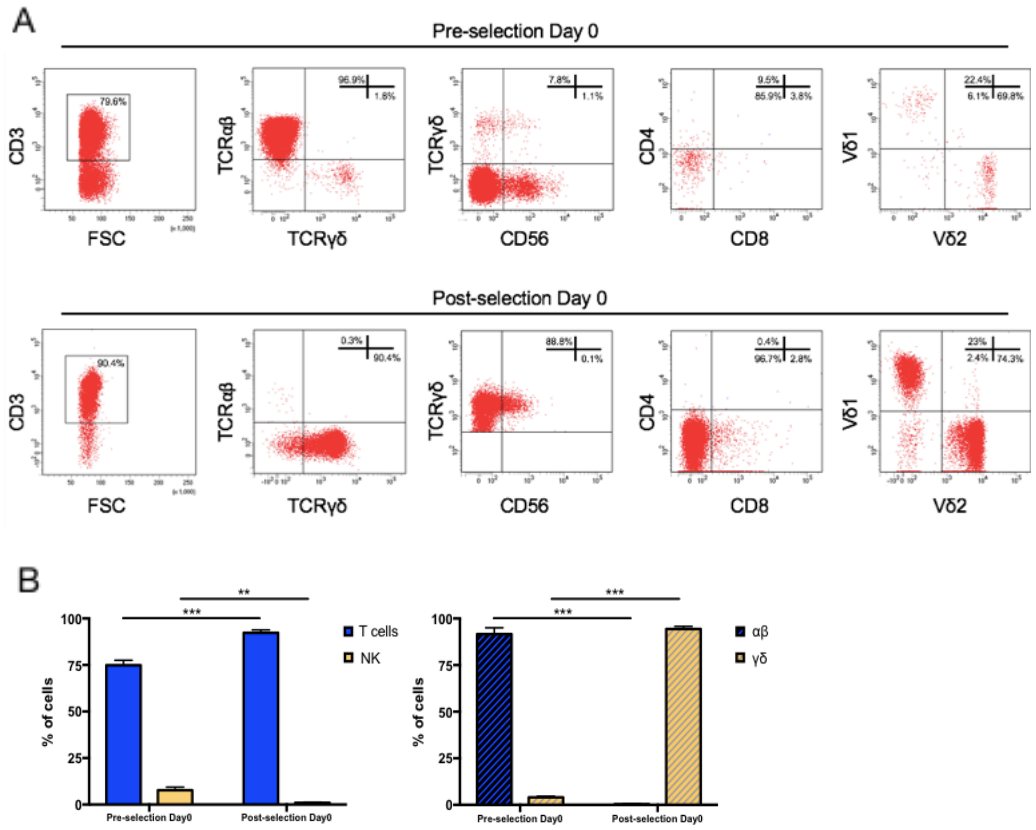

Figure 14: Purity on γδ-T cells recovery after selection from healthy donors. Human γδ-T cells were isolated from PBMCs using magnetic bead negative selection; the cellular composition was analysed by flow cytometry both before and after isolation (pre- and post-selection day 0) (A). The percentage of pre- and post-selection in T cells and NK cell composition, as well as in αβ and γδ-T-cells, is represented in panel B. Data from 4 donors are expressed as average ± SEM. *p<0.05; **p<0.01; ***p<0.001; **** p<0.0001.

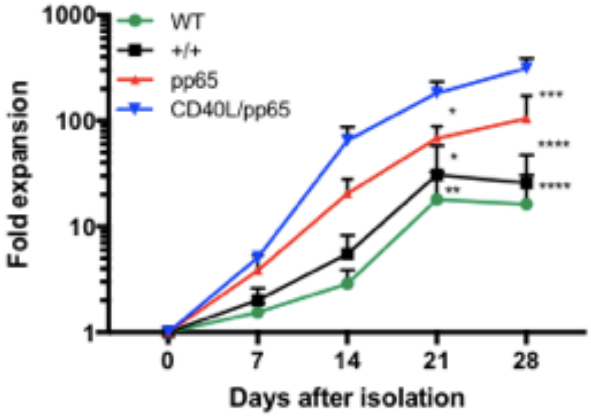

Figure 15: Fold expansion of γδ-T cells from healthy donors after stimulation with aAPCs. The fold expansion of isolated γδ-T cells co-cultured with each of the generated engineered aAPCs (+/+, pp65 and CD40L/pp65) and with WT aAPCs. Data from 4 donors are expressed as average ± SEM. *p<0.05; **p<0.01; ***p<0.001; **** p<0.0001.

A

DNA-System	K562 wt	γδ1-T_T0	γδ1-T_T28	γδ2-T_T0	γδ2-T_T28	γδ3-T_T0	γδ3-T_T28	γδ4-T_T0	γδ4-T_T28
AM	X, X	X, X	X, X	X, Y	X, Y	X, Y	X, Y	X, Y	X, Y
D6S1043	11, 15	11, 11	11, 11	12, 13	12, 13	12, 12	12, 12	13, 13	13, 13
Penta E	5, 14	10, 11	10, 11	7, 11	7, 11	11, 17	11, 17	7, 13	7, 13
D16S539	11, 12	12, 13	12, 13	9, 9	9, 9	9, 12	9, 12	11, 13	11, 13
D18S51	15, 16	13, 17	13, 17	12, 20	12, 20	17, 18	17, 18	15, 18	15, 18
Penta D	9, 13	11, 13	11, 13	7, 14	7, 14	10, 13	10, 13	13, 14	13, 14
D21S11	29, 31	30, 31.2	30, 31.2	26, 32.2	26, 32.2	29, 30	29, 30	31.2, 32.2	31.2, 32.2
D7S820	9, 11	10, 11	10, 11	9, 12	9, 12	9, 10	9, 10	9, 10	9, 10
D19S433	14, 14.2	13, 14.2	13, 14.2	13, 14	13, 14	14, 16	14, 16	13, 14	13, 14

B

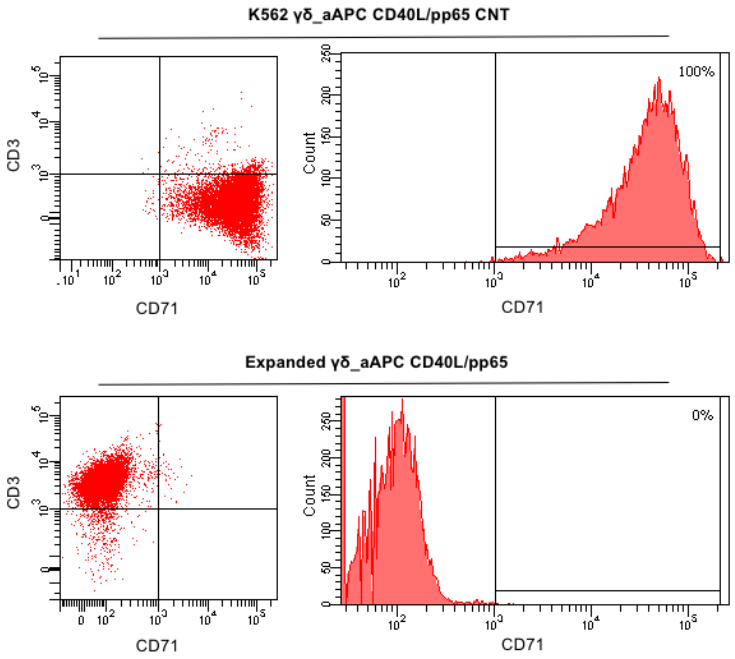

Figure 16: Identity of the expanded γδ-T cell products. At day+28 of expansion, CD40L/pp65 γδ-T cell products have been characterized in order to detect residual aAPCs. Short tandem repeat analysis was carried out on 4 different γδ-T cell products (**A**). Representative phenotype analysis for the detection of aAPC markers is shown in panel **B**.

3.8. CD40L/pp65 and pp65 aAPCs induce the expansion of polyclonal γδ-T cells with predominant Vδ1 phenotype.

γδ-T-cell products with the most efficient expansion (pp65 and CD40L/pp65) were phenotypically characterized at day+28. As shown in figure 17A, both products maintain purity (CD3/TCR-$\gamma\delta^{+}$) at the end of the expansion, with a maximum of 1.3%±0.8% and 1.9%±0.6% residual TCR-αβ T and NK cells, respectively; no statistical differences were observed between the two groups. At day+28, pp65-stimulated γδ-T cells maintained the same cell composition compared to that observed at the beginning of culture (90.6%±3.7% of $CD4^{neg}/CD8^{neg}$ and 3.4%±1.4% of $CD8^{+}$), whereas CD40L/pp65-stimulated cells significantly reduced the percentage of $CD4^{neg}/CD8^{neg}$, increasing the $CD8^{+}$ subset (40.2%±9% and 53.1%±8.6% respectively; $p<0.001$) (figure 17B). We then evaluated the polyclonality of our products, analysing the percentage of Vδ1, Vδ2 and $V\delta1^{neg}V\delta2^{neg}$ subsets within the $CD4^{+}$, $CD8^{+}$ and $CD4^{neg}/CD8^{neg}$ subpopulations: both $CD8^{+}$ and $CD4^{neg}/CD8^{neg}$ γδ-T populations revealed a significant enrichment of the Vδ1 compartment, especially in presence of CD40L costimulation ($p<0.001$). Only the $CD4^{+}$ subset, although fairly underrepresented, maintained a polyclonal phenotype (figure 17C).

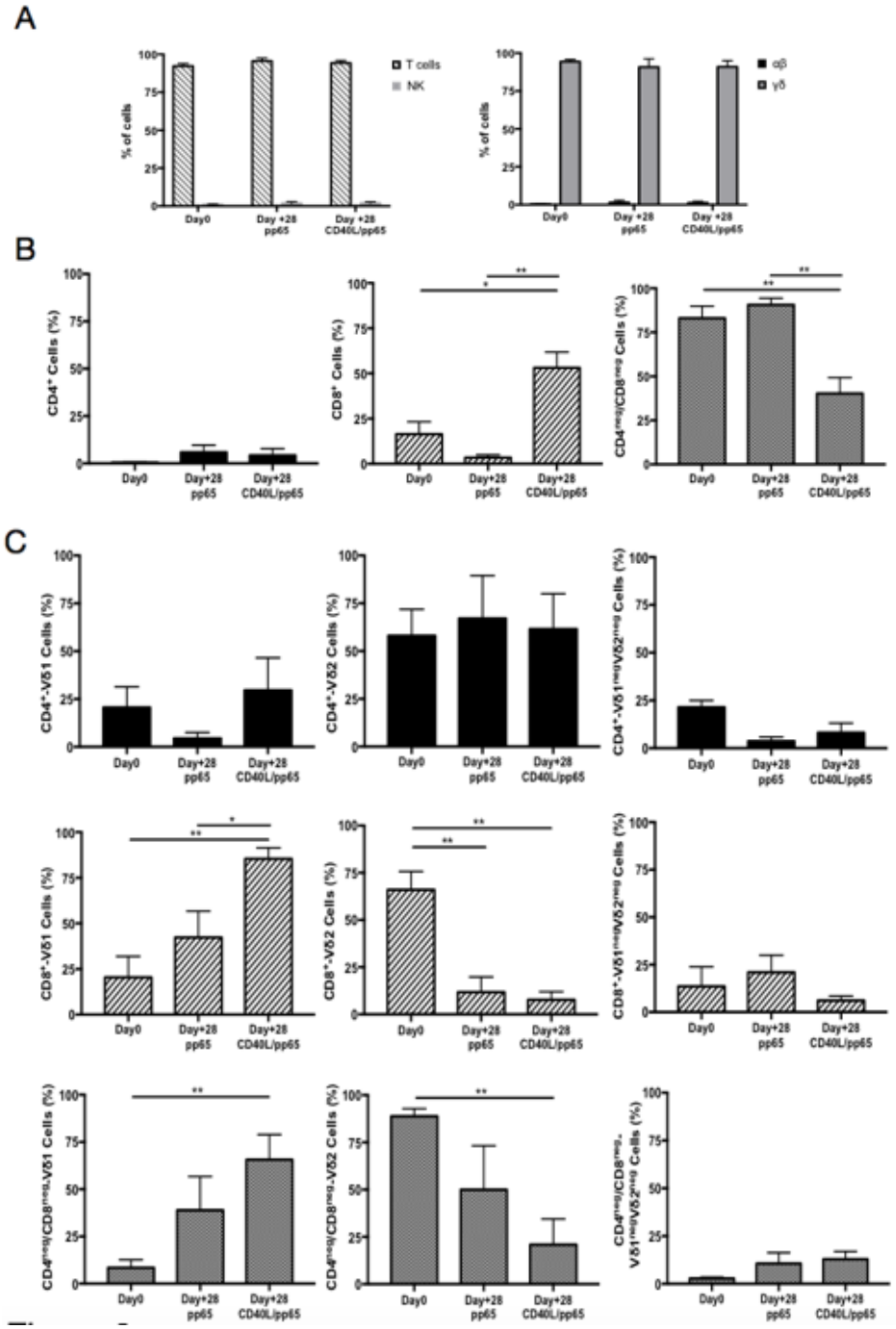

Figure 17: Phenotype of freshly isolated and expanded γδ-T cells stimulated with aAPCs/pp65 and CD40L/pp65.

Evaluation of T cells, NK cells, as well as of αβ and γδ-T cell subset distribution, in freshly isolated and expanded γδ-T cells (**A**). Panel **B** displays the flow cytometry analysis of the $CD4^{+}$, $CD8^{+}$ and $CD4^{neg}/CD8^{neg}$ cell content within the freshly isolated and expanded γδ-T cells. Distributions of Vδ1, Vδ2 and $Vδ1^{neg}Vδ2^{neg}$ subpopulations within the $CD4^{+}$, $CD8^{+}$ and $CD4^{neg}/CD8^{neg}$ in freshly isolated and expanded γδ-T cells are displayed in panels **C**. Data summarized as average ± SEM of 4 donors. *$p<0.05$; **$p<0.01$.

3.9. CD40L/pp65 costimulation of γδ-T cells maintains the memory phenotype without inducing overexpression of exhaustion markers.

Memory and exhaustion immunophenotypes of $CD4^+$, $CD8^+$ and $CD4^{neg}/CD8^{neg}$ γδ-T cells were analysed at day+28. In both pp65- and CD40L/pp65-expanded γδ-T cells a predominant percentage of central memory (CM, $CD45RO^+/CD27^+$) and effector memory (EfM, $CD45RO^+/CD27^-$) cells was observed (figure 18). To further characterize these γδ-T-cell populations, the expression of the activation marker CD95 and the activating/inhibitory receptors, PD1 and Lag3, were analysed to define the exhaustion profile. All the subsets showed high levels of CD95 expression, underlining their activated status. The analysis of PD1 and Lag3 revealed, instead, that although Lag3 levels were extremely high and homogeneous in the $CD4^+$ and $CD8^+$ subsets, in $CD4^{neg}/CD8^{neg}$ the expression was more heterogeneous. On the other hand, the level of PD1 was homogeneously low in the $CD8^+$ and $CD4^{neg}/CD8^{neg}$ subpopulations. Taken together, these markers suggest the presence of an activated, but not exhausted phenotype in these subpopulations. In the $CD4^+$ subset, however, the higher and heterogeneous expression of PD1 on the cells, which co-express Lag3, indicates an activated, but also more exhausted phenotype (figure 18).

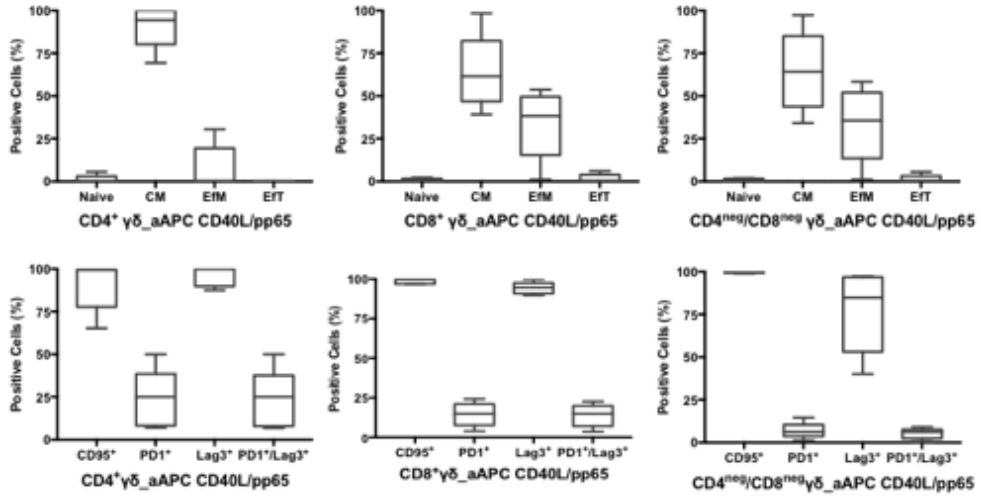

Figure 18: Phenotype of expanded γδ-T cells. Characterization of the effector/memory, activation and exhaustion profile of CD40L/pp65 expanded γδ-T cells in the $CD4^+$, $CD8^+$ and $CD4^{neg}/CD8^{neg}$ subpopulations.

3.10. Expanded γδ-T cells can penetrate into the hydrogel and reach the tumor organoids.

Expanded γδ-T cells were then analysed for their functional anti-tumour activity using conventional long-term co-culture assays as well as in our established 3D model. In detail, polyclonally activated and expanded αβ-T cells, used as conventional control, or CD40L/pp65-stimulated γδ-T were co-cultured for 6 and 14 days with either U87-GFP+ or U373-GFP+ cells at an E:T ratio of 1:1 in 2D and 3D platforms. After 6 days of co-culture with U87 GFP+, expanded γδ-T cells in 2D showed a significantly higher cytotoxic activity, compared to expanded αβ-T cells ($p=0.0229$), whose activity, however, is driven by alloreactivity (figure 19A). While, in the 3D model after 6 days of co-culture there is no significant difference between the αβ-T cells and CD40L/pp65-stimulated γδ-T activity

even though a trend is detectable in favour of activated and expanded γδ-T cells (figure 19A). It is important to underline that the effects of alloreactivity observed in the 2D model are completely abrogated in the 3D system. The same experiments were then carried out until 14 day. Only 3D cultures were able to be analysed at that time point due to the fact the all the cells in 2D cultures were completely necrotic. We observed that the anti-tumor activity was maintained in the γδ-T cell treated condition conserving a significant difference compared to αβ-T cells (p=0.0009) (figure 19B). Also, in this case, our experiments demonstrate clearly that there is a significant difference between 2D and 3D models after 6 days of co-culture (αβ-T cells: p=0.0121; CD40L/pp65-stimulated γδ-T: p=0.0009) (figure 19A). Instead, when we repeated the experiments using the less aggressive U373 cell line, no substantial difference between the two models was observed (figure 19C); however, a trend in tumor reduction was clearly observed in the 3D model at 14 days of co-culture (figure 19D). In summary, all together these results show how in the 3D model the structure assumed by the tumor and the cellular organization leads to a later response to the treatments, closer to what happens *in-vivo*.

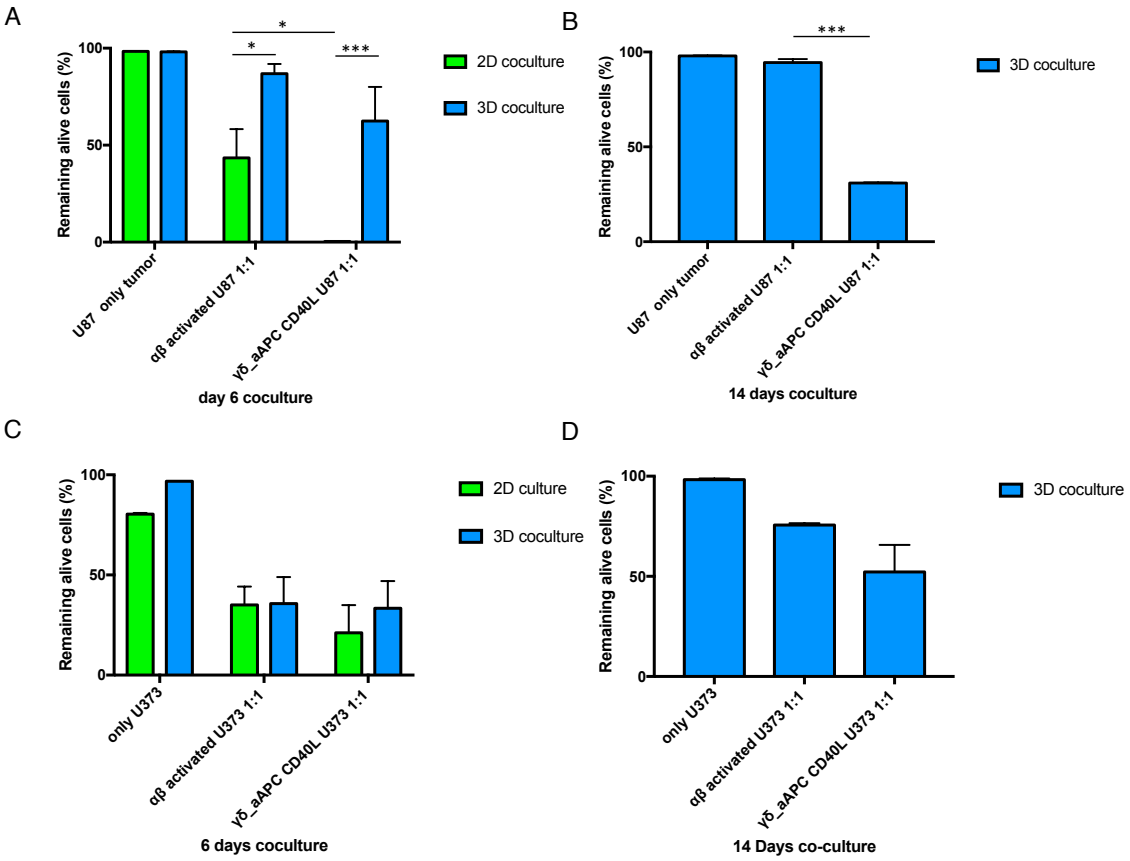

Figure 19: Anti-tumour activity of expanded αβ-T and γδ-T cells in long-term in vitro assays in 2D and 3D models. The histograms in the figure show the residual percentage of tumors (U87 and U373) in 2D and 3D models after 6 days of co-culture with αβ-T cells or CD40L/pp65-stimulated γδ-T (**A and C**) and after 14 days of co-culture in the 3D model (**B and D**).

DISCUSSION

Gliomas are a heterogeneous group of tumors that arise within the brain parenchyma and which have been classified by the World Health Organization in subgroups based on histopathological characteristics and specific molecular markers that recapitulate the prognosis [91]. The term "glioma" refers to tumors that have histologic features similar to normal glial cells like astrocytes, oligodendrocytes and ependymal cells. Patients affected by slower-growing lesions (grade I and II), commonly referred to as LGGs, show a longer survivorship than those with more rapidly progressive tumors (grade III and IV) named High Grade Gliomas [92]. Up to date treatment for LGG consists of surgery and other conventional therapies such as chemotherapy and radiotherapy. However, the localization and the size of the mass often make surgery extremely difficult. Furthermore, it is important to underline that in many of these patients, due to the treatments they undergo, the quality of life is highly compromised. For these reasons, it is crucial to find new and more promising strategies capable to fight the tumor, reduce toxicity and improve the quality of life, such as immunotherapy and targeted therapies [93]. Furthermore, since LGG are solid tumors, the behavior of tumor cells and the response to therapies is strongly influenced by their tumor microenvironment [94]. Several earlier studies clearly demonstrate how the 3D organization of tumor cells is essential to recapitulate and regulate tumor characteristics and behavior [95-96]. The 3D network and the cellular context allow the establishment of interactions both physically and biochemically capable of modifying key events of cell biology and alter tissue growth and homeostasis [95-97].

Therefore, it is important to develop a model that recapitulates the tumor microenvironment and reproduces the architecture of the tumor itself [98]. The common bi-dimensional (2D) culture systems are not able to faithfully reproduce the structural complexity, the organization and the cellular interactions between the tumor cells and the various components of the tumor microenvironment [99]. Thus, 2D systems are often not predictive of the real efficacy of different therapies in preclinical studies, especially in the case of complex approaches such as immunotherapy. Furthermore, with particular reference to LGG, it is difficult to identify and test the efficacy of therapies due to the well-known activation of senescence pathways in primary cultured tumor cells [7] which inhibits the generation of immortalized cell lines. In this study, we used a 3D model based on a PEG-fibrin hydrogel that overcomes this limit[88], allowing the realization of long-term cultures and the creation of organoids that reproduce the characteristics of the primary tumors representing an optimal platform for the study and realization of stable LGG cell lines. This model may provide a more accurate prediction of responses and sensitivity to drugs and radiotherapy than 2D cultures. These differences may be accentuated in the study of more complex biological therapies, which may be even more dependent on the physical arrangement and surface phenotype of malignant cells [100-101]. The 3D hydrogel culture system that we developed has several practical advantages over commercially available 3D scaffolds in terms of production and handling. We chose fibrin, a minor component of the tumor extra-cellular matrix (ECM), over other more predominant ECM proteins such as collagen because we wished to provide only an initial structural support for the 3D tumor to form its own matrix; the enzymatic digestion with a low-cost protease recovers almost all the cells as a single cell suspension even after long-term culture and without altering their phenotype. Standard *in vitro* techniques can be applied to the

study of these cultures, including microscopic monitoring (bright field and fluorescence), quantitative monitoring through bioluminescence, flow cytometry on vital cells after enzymatic digestion, and histologic analysis after paraffin embedding. The high stability over time of the PEG-fibrin hydrogel represents another advantage over the use of ECM components such as collagen, since the latter can be degraded by tumors with high metastatic abilities, thereby impairing the function of a component that is required for long-term co-cultures. All these features make the PEG-fibrin hydrogel a highly attractive platform for *in vitro* and *in vivo* modeling of tumor-stromal interaction and enable its use in studies of the response to biological treatments in a controlled fashion. In these PEG-fibrin hydrogels, tumor cells organize into organoids that more closely recapitulate the *in vivo* phenotype and growth kinetics of human LGG, and tumors cultured in this model should therefore provide a more accurate prediction of potency and efficacy of tested agents [102]. Two-dimensional cultures can offer only limited information about tumor-stromal cell interactions, since the complex architecture of the tumor cannot be reproduced and long-term co-cultures are impossible to maintain without passaging the cells, disrupting cell-to-cell interactions, and impeding cellular crosstalk. In this study, we demonstrated that the 3D model, thanks to its ability to maintain tumor microenvironment and support its organization, allows the development of primary LGG cultures deriving from pediatric patients, evading activation of senescence pathway, which are normally activated in the primary lines of LGG in a conventional two-dimensional system [7] making the development of stable lines difficult and consequently functional *in-vitro* cellular model. All the primary 3D lines show a significant and consistantly lower expression of beta-galactosidase compared to the matched canonical 2D cultures. These data was then confirmed by the analysis of other markers that were previously reported as signs of senescence in LGG. In our 3D

model, we observed high levels of the proliferating marker Ki-67 and a reduction of p16 expression, while in the 2D culture we confirmed the low expression of Ki-67 and high level of p16 as previously demonstrated by other groups [103-104], indicating the activation of senescence pathways. This demonstrates how the 3D system is an optimal platform to develop primary LGG cultures that can be used to test conventional therapies such as chemotherapy and radiotherapy, but also to test and evaluate the response to more complex therapies such as immunotherapies like oncolytic viruses and adoptive T cell transfer. Therefore, we evaluated the antitumor activity of an innovative immunotherapeutic approach based on the use of γδ-T cells. These cells can represent a potentially novel and effective immunotherapeutic approach for the treatment of cancers because of their innate cytotoxicity [19], against virally infected cells and tumors, their physiological capacity to infiltrate inside the tumor microenvironment of solid malignancies as well as for their potential to be used in an allogeneic setting without causing toxicity [21]. Furthermore, several reports underline the role of γδ-T cells in boosting the response of the immune system due to their professional antigen presenting cell (APCs) propriety [22]. In this study, we developed a clinical-grade protocol to isolate and efficiently expand, both manually and automatically, high numbers of polyclonal γδ-T cells. The cellular products generated were highly stable over time, maintaining a polyclonal and memory phenotype and an excellent anti-tumor response. Due to the limited capacity to expand this population in vitro with the conventional protocols, we explored the possibility to activate and expand them using artificial APC (aAPC). The introduction of the costimulatory molecules CD86, 4-1BBL, CD40L and pp65-CMV antigen on aAPCs allowed a great expansion of γδ-T cells. Moreover, while maintaining a polyclonal phenotype, a major representation of the memory infiltrating Vδ1 subgroup was observed in

our system. The polyclonal cellular product obtained display an extensive anti-tumor activity. In view of potential safety concerns associated with the use of irradiated tumor cells as feeders, we further engineered the aAPCs with the inducible suicide gene Caspase 9 (iC9) as safety switch, whose efficacy has already been validated in several clinical trials(20). The possibility of using tumor cell lines as feeder cells is supported by several on-going clinical studies (NCT00694330, NCT00361296, NCT00363649) [105]. Lastly, we characterized the anti-tumor activity of expanded and activated γδ-T cells, and of more conventional approaches such as radiotherapy and chemotherapy, in both 2D and in 3D-cultured tumors. The results clearly show, in both culture conditions, the higher power of the expanded γδ-T cells to eliminate tumor cells compared to conventional therapies. The data obtained with chemo- and radiotherapy recapitulates what is being observed in vivo in-patient treatment. These data suggest a more realistic estimation of the efficacy of such advanced treatments in the 3D-platform, confirming it to be a better model for biological and therapeutic studies. The 3D platform proved to be more reliable in terms of predictive power compared to two-dimensional cultures. The same cells grown in 2D and in 3D have different morphology, organization and proliferative rate; all these differences influence the biological behavior and the response to the various treatments. In fact, while in 2D we have a remarkable response to various treatments with a complete eradication of the tumor after few days, in 3D the response varies depending on the treatment and the specific conditions. Cells grown in 3D respond to therapies in longer times than the same grown in 2D, showing how this model provides a more realistic situation than what happens *in-vivo*, where normally the effect is visible after many days. In conclusion, our study shows that PEG-fibrin hydrogel can support the development of LGG primary cultures and has several potential advantages over other 3D

systems. PEG-hydrogels provide a means for testing advanced immunotherapeutic approaches such as monoclonal antibodies, oncolytic viruses and adoptive T cell transfer for cancer treatment, helping to reduce the need for complex and extensive animal models and also overcome the intrinsic limitations of xenograft and other models.

Work limitation

One of the advances of the strategy suggested in this study, which is based on pegylated fibrin hydrogels, is that they are a lot less expensive than any murine model and have significant ethical advantages in terms both of number of mice used and procedures which these animals must undergo. We prove that 3D models are optimal for the preliminary study of complex therapies, since they recapitulate important aspects of *in vivo* tumors, however it is important to underline that they have some limitations. Though the 3D model we use is more predictive from the point of view of the response than the 2D, it is much more time-consuming and certainly more expensive than the classic 2D models. Even with respect to murine models, 3D presents limits, in fact it can be considered as an intermediate model between the 2D platform and the *in vivo* model. The 3D, in fact, fails to recapitulate the systemic complexity of a complex organism such as the mouse. However, it can be useful to considerably reduce the use of a large number of animals. In the setting of LGG, the 3D models is also able to sustain the generation of a more representative tumor that can be used for the generation of mouse models and test therapeutic options, thanks to its heterogeneity in cellular composition.

Furthermore, we decided to investigate the possibility to use γδ-T cells for the treatment of LGG or in general of other brain tumor because we wanted to exploit the intrinsic capabilities of this particular population of our innate immune system to generate a cellular product with anti-tumor properties that can be used even in an allogeneic setting thanks to their complete absence of allogeneity. The basic idea is to generate a third-party T cell bank from non-correlated donors as an off-the-shelf and ready-to-use product.

Using this population we do not expect to reach a complete eradication of the tumor *in vivo* in patients, but the use of the 3D platform can be a useful tool to better address the potentiality of this immunotherapeutic approach as well as of others such as oncolytic viruses, monoclonal antibodies, natural killer cells or αβ/γδ T cells armed with chimeric antigen receptors.

REFERENCES

1. Louis DN, Ohgaki H, Wiestler OD, et al. The 2007 WHO classi- fication of tumours of the central nervous system. Acta Neuro- pathol. 2007;114(2):97-109.

2. Louis DN, Perry A, Burger P, et al. International Society of Neuropathology—Haarlem consensus guidelines for nervous system tumor classification and grading. Brain Pathol. 2014;24(5): 429-435.

3. Ostrom QT, Gittleman H, Liao P, et al. CBTRUS statistical report: primary brain and central nervous system tumors diag- nosed in the United States in 2007-2011. Neuro-oncol. 2014;16(suppl 4):1-63.

4. Bigner SH, McLendon RE, Fuchs H, McKeever PE, Friedman HS. Chromosomal characteristics of childhood brain tumors. Cancer Genet Cytogenet. 1997;97(2):125-134.

5. Analysis.Y.Y. Wang, T. Zhang, S.W. Li, T.Y. Qian, X. Fan, X.X. Peng, J. Ma, L. Wang and T. Jiang. Mapping p53 Mutations in Low-Grade Glioma: A Voxel-Based Neuroimaging American Journal of Neuroradiology January 2015, 36 (1) 70-76;

6. Yoshiko Okita, Yoshitaka Narita,Yasuji Miyakita,Makoto Ohno, Yuko Matsushita, Shintaro Fukushima, Minako Sumi, Koichi Ichimura, Takamasa Kayama, Soichiro Shibui. IDH1/2 mutation is a prognostic marker for survival and predicts response to chemotherapy for grade II gliomas concomitantly treated with radiation therapy. International Journal of Oncology. July 20, 2012. 1325-1336.

7. Eric H. Raabe, Kah Suan Lim, Julia M. Kim, Alan Meeker, Xing-gang Mao, Guido Nikkhah, Jarek Maciaczyk, Ulf Kahlert, Deepali Jain, Eli Bar, Kenneth J. Cohen, and Charles G. Eberhart. BRAF Activation Induces Transformation and Then Senescence in Human Neural Stem Cells: A Pilocytic Astrocytoma Model. Clin Cancer Re. 2011 June1.17(11):3590-3599

8. Pollack IF, Finkelstein SD, Burnham J, et al. Age and TP53 muta- tion frequency in childhood malignant gliomas: results in a multi- institutional cohort. Cancer Res. 2001;61(20):7404-7407.

9. Yan H, Parsons DW, Jin G, et al. IDH1 and IDH2 mutations in gliomas. N Engl J Med. 2009;360(8):765-773.

10. Wisoff JH, Sanford RA, Heier LA, et al. Primary neurosurgery for pediatric low-grade gliomas: a prospective multi-institutional study from the Children's Oncology Group. Neurosurg. 2011; 68(6):1548-1554, discussion 1554-1555.

11. Benesch M, Eder HG, Sovinz P, et al. Residual or recurrent cer- ebellar low-grade glioma in children after tumor resection: is re-treatment needed? A single center experience from 1983 to 2003. Pediatr Neurosurg. 2006;42(3):159-164.

12. Ater JL, Zhou T, Holmes E, et al. Randomized study of two che- motherapy regimens for treatment of low-grade glioma in young children: a report from the Children's Oncology Group. J Clin Oncol. 2012;30(21):2641-2647.

13. Bouffet E, Jakacki R, Goldman S, et al. Phase II study of weeklyvinblastine in recurrent or refractory pediatric low-grade glioma.J Clin Oncol. 2012;30(12):1358-1363.

14. Ruella M, Kalos M. Adoptive immunotherapy for cancer. Immunol Rev. 2014 Jan;257(1):14-38.

15.Leung W, Hudson MM, Strickland DK, Phipps S, Srivastava DK, Ribeiro RC, et al. Late effects of treatment in survivors of childhood acute myeloid leukemia. J Clin Oncol (2000) 18(18):3273-9. Epub 2000/09/14. doi: 10.1200/JCO.2000.18.18.3273. PubMed PMID: 10986060.

16.Sahin U, Toprak SK, Atilla PA, Atilla E, Demirer T. An overview of infectious complications after allogeneic hematopoietic stem cell transplantation. J Infect Chemother (2016) 22(8):505-14. Epub 2016/06/28. doi: 10.1016/j.jiac.2016.05.006. PubMed PMID: 27344206.

17.Born W, Miles C, White J, O'Brien R, Freed JH, Marrack P, Kappler J, Kubo RT. Peptide sequences of T-cell receptor delta and gamma chains are identical to predicted X and gamma proteins. Nature. 1987;330:572–4.

18. Holtmeier W, Kabelitz D. γδ T cells link innate and adaptive immune responses. In: Kabelitz D, Schröder JM, editors. Mechanisms of epithelial defense, vol. 86. Basel: Karger Publishers; 2005. p. 151–83.

19. Vantourout P, Hayday A. Six-of-the-best: unique contributions of gammadelta T cells to immunology. Nat Rev Immunol (2013) 13(2):88-100. Epub 2013/01/26. doi: 10.1038/nri3384.PubMed PMID: 23348415; PubMed Central PMCID: PMCPMC3951794.

20. Dar AA, Patil RS, Chiplunkar SV. Insights into the relationship between toll like receptors and gamma delta t cell responses. Front Immunol. 2014;5:366.

21.Gentles AJ, Newman AM, Liu CL, Bratman SV, Feng W, Kim D, et al. The prognostic landscape of genes and infiltrating immune cells across human cancers. Nat Med. 2015;21(8):938-45.

22.Khan MW, Curbishley SM, Chen HC, Thomas AD, Pircher H, Mavilio D, et al. Expanded Human Blood-Derived gammadeltaT Cells Display Potent Antigen-Presentation Functions. Front Immunol. 2014;5:344.

23. Niu C, Jin H, Li M, Xu J, Xu D, Hu J, et al. In vitro analysis of the prolifera- tive capacity and cytotoxic effects of ex vivo induced natural killer cells, cytokine-induced killer cells, and gamma-delta T cells. BMC Immunol. 2015;16:61.

24. Viey E, Fromont G, Escudier B, Morel Y, Da Rocha S, Chouaib S, et al. Phosphostim-activated γδ T cells kill autologous metastatic renal cell carcinoma. J Immunol. 2005;174:1338–47.

25.Kang N, Zhou J, Zhang T, Wang L, Lu F, Cui Y, et al. Adoptive immunotherapy of lung cancer with immobilized anti-TCRgammadelta antibody-expanded human gammadelta T-cells in peripheral blood. Cancer Biol Ther (2009) 8(16):1540-9. Epub 2009/05/28. PubMed PMID: 19471115.

26.Fournie JJ, Sicard H, Poupot M, Bezombes C, Blanc A, Romagne F, et al. What lessons can be learned from gammadelta T cell-based cancer immunotherapy trials? Cell Mol Immunol (2013) 10(1):35-41. Epub 2012/12/18. doi: 10.1038/cmi.2012.39. PubMed PMID: 23241899; PubMed Central PMCID: PMCPMC4003170.

27.Godder KT, Henslee-Downey PJ, Mehta J, Park BS, Chiang KY, Abhyankar S, et al. Long term disease-free survival in acute leukemia patients recovering with increased gammadelta T cells after partially mismatched related donor bone marrow transplantation. Bone Marrow Transplant (2007) 39(12):751-7. doi: 10.1038/sj.bmt.1705650. PubMed PMID: 17450185.

28.Airoldi I, Bertaina A, Prigione I, Zorzoli A, Pagliara D, Cocco C, et al. gammadelta T-cell reconstitution after HLA-haploidentical hematopoietic transplantation depleted of TCR-alphabeta+/CD19+ lymphocytes. Blood (2015) 125(15):2349-58. Epub 2015/01/24. doi: 10.1182/blood-2014-09-599423. PubMed PMID: 25612623; PubMed Central PMCID: PMCPMC4440890.

29.Dimova T, Brouwer M, Gosselin F, Tassignon J, Leo O, Donner C, et al. Effector Vgamma9Vdelta2 T cells dominate the human fetal gam- madelta T-cell repertoire. Proc Natl Acad Sci USA. 2015;112:E556–65.

30.Di Carlo E, Bocca P, Emionite L, Cilli M, Cipollone G, Morandi F, et al. Mechanisms of the antitumor activity of human Vgamma9Vdelta2 T cells in combination with zoledronic acid in a preclinical model of neuroblastoma. Mol Ther. 2013;21:1034–43.

31.Braza MS, Klein B. Anti-tumour immunotherapy with Vgamma9Vdelta2 T lymphocytes: from the bench to the bedside. Br J Haematol. 2013;160:123–32.

32.Almeida AR, Correia DV, Fernandes-Platzgummer A, da Silva CL, da Silva MG, Anjos DR, et al. Delta one T cells for immunotherapy of chronic lymphocytic leukemia: clinical-grade expansion/differentiation and preclinical proof of concept. Clin Cancer Res. 2016;22:5795–804.

33.Godder KT, Henslee-Downey PJ, Mehta J, Park BS, Chiang KY, Abhyankar S, et al. Long-term disease-free survival in acute leukemia patients recovering with increased gammadelta T cells after partially mismatched related donor bone marrow transplantation. Bone Marrow Transplant. 2007;39(12):751-7.

34.Knight A, Arnouk H, Britt W, Gillespie GY, Cloud GA, Harkins L, et al. CMV-independent lysis of glioblastoma by ex vivo expanded/activated Vdelta1+ gammadelta T cells. PLoS One. 2013;8(8):e68729.

35. Bonneville M, O'Brien RL, Born WK. Gammadelta T cell effector functions: a blend of innate programming and acquired plasticity. Nat Rev Immunol (2010) 10(7):467-78. Epub 2010/06/12. doi: 10.1038/nri2781. PubMed PMID: 20539306.

36.Siegers GM, Lamb LS, Jr. Cytotoxic and regulatory properties of circulating Vdelta1+ gammadelta T cells: a new player on the cell therapy field? Mol Ther. 2014;22(8):1416-22.

37.Willcox CR, Pitard V, Netzer S, Couzi L, Salim M, Silberzahn T, et al. Cytomegalovirus and tumor stress surveillance by binding of a human gammadelta T cell antigen receptor to endothelial protein C receptor. Nat Immunol. 2012;13(9):872-9.

38.Deniger DC, Maiti SN, Mi T, Switzer KC, Ramachandran V, Hurton LV, et al. Activating and propagating polyclonal gamma delta T cells with broad specificity for malignancies. Clin Cancer Res. 2014;20(22):5708-19.

39.Morita CT, Tanaka Y, Bloom BR, Brenner MB. Direct presentation of non-peptide prenyl pyrophosphate antigens to human gamma delta T cells. Res Immunol (1996) 147(5):347-53. Epub 1996/06/01. PubMed PMID: 8876064.

40.Devilder MC, Maillet S, Bouyge-Moreau I, Donnadieu E, Bonneville M, Scotet E. Potentiation of antigen-stimulated V gamma 9V delta 2 T cell cytokine production by immature dendritic cells (DC) and reciprocal effect on DC maturation. J Immunol (2006) 176(3):1386-93. Epub 2006/01/21. PubMed PMID: 16424165.

41.Conti L, Casetti R, Cardone M, Varano B, Martino A, Belardelli F, et al. Reciprocal activating interaction between dendritic cells and pamidronate-stimulated gammadelta T cells: role of CD86 and inflammatory cytokines. J Immunol (2005) 174(1):252-60. Epub 2004/12/22. PubMed PMID: 15611247.

42.Lopez RD, Xu S, Guo B, Negrin RS, Waller EK. CD2-mediated IL-12-dependent signals render human gamma delta-T cells resistant to mitogen-induced apoptosis, permitting the large-scale ex vivo expansion of functionally distinct lymphocytes: implications for the development of adoptive immunotherapy strategies. Blood (2000) 96(12):3827-37. Epub 2000/11/23. PubMed PMID: 11090067.

43.Lamb LS, Jr., Gee AP, Hazlett LJ, Musk P, Parrish RS, O'Hanlon TP, et al. Influence of T cell depletion method on circulating gammadelta T cell reconstitution and potential role in the graft-versus-leukemia effect. Cytotherapy (1999) 1(1):7-19. Epub 1999/01/01. PubMed PMID: 19746645.

44.Pressey JG, Adams J, Harkins L, Kelly D, You Z, Lamb LS, Jr. In vivo expansion and activation of gammadelta T cells as immunotherapy for refractory neuroblastoma: A phase 1 study. Medicine (Baltimore) (2016) 95(39):e4909. Epub 2016/09/30. doi: 10.1097/MD.0000000000004909. PubMed PMID: 27684826; PubMed Central PMCID: PMCPMC5265919.

45.Kondo M, Sakuta K, Noguchi A, Ariyoshi N, Sato K, Sato S, et al. Zoledronate facilitates large-scale ex vivo expansion of functional gammadelta T cells from cancer patients for use in adoptive immunotherapy. Cytotherapy (2008) 10(8):842-56. Epub 2008/11/20. doi: 10.1080/14653240802419328. PubMed PMID: 19016372.

46.Lang JM, Kaikobad MR, Wallace M, Staab MJ, Horvath DL, Wilding G, et al. Pilot trial of interleukin-2 and zoledronic acid to augment gammadelta T cells as treatment for patients with refractory renal cell carcinoma. Cancer Immunol Immunother (2011) 60(10):1447-60. Epub 2011/06/08. doi: 10.1007/s00262-011-1049-8. PubMed PMID: 21647691; PubMed Central PMCID: PMCPMC3177972.

47.Capsomidis A, Benthall G, Van Acker HH, Fisher J, Kramer AM, Abeln Z, et al. Chimeric Antigen Receptor-Engineered Human Gamma Delta T Cells: Enhanced Cytotoxicity with Retention of Cross Presentation. Mol Ther (2018) 26(2):354-65. Epub 2018/01/10. doi: 10.1016/j.ymthe.2017.12.001. PubMed PMID: 29310916; PubMed Central PMCID: PMCPMC5835118.

48.Siegers GM, Dhamko H, Wang XH, Mathieson AM, Kosaka Y, Felizardo TC, et al. Human Vdelta1 gammadelta T cells expanded from peripheral blood exhibit specific cytotoxicity against B-cell chronic lymphocytic leukemia-derived cells. Cytotherapy (2011) 13(6):753-64. Epub 2011/02/15. doi: 10.3109/14653249.2011.553595. PubMed PMID: 21314241.

49.Deniger DC, Maiti SN, Mi T, Switzer KC, Ramachandran V, Hurton LV, et al. Activating and propagating polyclonal gamma delta T cells with broad specificity for malignancies. Clin Cancer Res (2014) 20(22):5708-19. Epub 2014/05/17. doi: 10.1158/1078-0432.CCR-13-3451. PubMed PMID: 24833662; PubMed Central PMCID: PMCPMC4233015.

50.Yamada K, Cukierman E. Modeling tissue morphogenesis and cancer in 3D. Cell 2007; 130: 601-10.

51.Jacoby W, Pasten I. Methods in Enzymology: Cell Culture. Vol. 58. Academic Press, New York 1979.

52.Sanyal S. Culture and assay systems used for 3D cell culture. Corning 2014; 9: 1-18.

53.Aggarwal B, Danda D, Gupta S, Gehlot P. Models for prevention and treatment of cancer: problems vs promises.Biochem Pharmacol 2009; 78: 1083-94.

54.Pampaloni F, Reynaud EG, Stelzer EH. The third dimension bridges the gap between cell culture and live tissue. Nat Rev Mol Cell Biol 2007; 8: 839-45.

55.Breslin S, O'Driscoll L. Three-dimensional cell culture: the missing link in drug discovery. Drug Discov Today 2013; 18: 240-9.

56.Baker B, Chen C. Deconstructing the third dimension how 3D culture microenvironments alter cellular cues.J Cell Sci 2012; 125: 3015-24.

57.Bissell MJ, Rizki A, Mian IS. Tissue architecture: the ul- timate regulator of breast epithelial function. Curr Opin Cell Biol 2003; 15: 753-62.

58.Mahmud G, Campbell CJ, Bishop KJM, et al. Directing cell motions on micropatterned ratchets. Nat Phys 2009; 5: 606-12.

59. Kilian K, Bugarija B, Lahn BT, et al. Geometric cues for directing the differentiation of mesenchymal stem cells. Proc Natl Acad Sci USA 2010; 107: 4872-7.

60.Mseka T, Bamburg JR, Cramer LP. ADF/cofilin family pro- teins control formation of oriented actin-filament bun- dles in the cell body to trigger fibroblast polarization. J Cell Sci 2007; 120: 4332-44.

61.Weaver V, Lelièvre S, Lakins JN, et al. Beta4 integrin-de- pendent formation of polarized three-dimensional ar- chitecture confers resistance to apoptosis in normal and malignant mammary epithelium. Cancer Cell 2002; 2: 205-16.

62. Meyers J, Craig J, Odde DJ. Potential for control of sig- naling pathways via cell size and shape. Curr Biol 2003; 16: 1685-93.

63.Birgersdotter A, Sandberg R, Ernberg I. Gene expression perturbation in vitro – a growing case for three-dimen- sional (3D) culture systems. Semin Cancer Biol 2005; 15: 405-12.

64.Gomez-Lechon M, Jover R, Donato T, et al. Long-term expression of differentiated functions in hepatocytes cultured in three-dimensional collagen matrix. J Cell Physiol 1998; 77: 553-62.

65.Hamburger A, Salmon SE. Primary bioassay of human tumor stem cells. Science 1977; 197: 461-3.

66.Griffith LG, Swartz MA. Capturing complex 3D tissue physiology in vitro. Nat Rev Mol Cell Biol 2006; 7: 211-24.

67.Cawkill D, Eaglestone SS. Evolution of cell-based reagent provision. Drug Discov Today 2007; 12: 820-5.

68.Lee J, Cuddihy MJ, Kotov NA. Three-dimensional cell culture matrices: state of the art. Tissue Eng Part B Rev 2008; 14: 61-86.

69.Petersen OW, Rønnov-Jessen L, Howlett AR, Bissel MJ. Interaction with basement membrane serves to rapidly distinguish growth and differentiation pattern of nor- mal and malignant human breast epithelial cells. Proc Natl Acad Sci USA 1992; 89: 9064-8.

70. Benya PD, Shaffer JD. Dedifferentiated chondrocytes reexpress the differentiated collagen phenotype when cultured in agarose gels. Cell 1982; 30: 215-24.

71. Pradhan-Bhatt S, Harrington DA, Duncan RL, et al. A nov- el in vivo model for evaluating functional restoration of a tissue-engineered salivary gland. Laryngoscope 2014; 124: 456-61.

72. Pradhan-Bhatt S, Harrington DA, Duncan RL, Jia X, Witt RL, Farach-Carson MC. Implantable three-dimen- sional salivary spheroid assemblies demonstrate fluid and protein secretory responses to neurotransmitters. Tissue Eng Part A 2013; 19: 1610-20.

73. Ghosh S, Spagnoli GC, Martin I, et al. Three-dimensional culture of melanoma cells profoundly affects gene ex- pression profile: a high density oligonucleotide array study. J Cell Physiol 2005; 204: 522-31.

74. Marushima H, Shibata S, Asakura T, et al. Three-di- mensional culture promotes reconstitution of the tu- mor-specific hypoxic microenvironment under TGFβ stimulation. Int J Oncol 2011; 39: 1327-36.

75.M.J. Bissell, D. Radisky,. Putting tumours in context, Nat. Rev. Cancer 1 (2001)46e54.

76.F. Pampaloni, E.G. Reynaud, E.H.K. Stelzer, The third dimension bridges the gap between cell culture and live tissue, Nat. Rev. Mol. Cell Biol. 8 (2007)839e845.

77.D.W. Hutmacher, Biomaterials offer cancer research the third dimension, Nat.Mater 9 (2010) 90e93.

78.L.C. Kimlin, G. Casagrande, V.M. Virador, In vitro three-dimensional (3D) models in cancer research: an update, Mol. Carcinog. 52 (2013) 167e182.

79. S. Ghosh, G.C. Spagnoli, I. Martin, S. Ploegert, P. Demougin, M. Heberer,A. Reschner, Three-dimensional culture of melanoma cells profoundly affects gene expression profile: a high density oligonucleotide array study, J. Cell Physiol. 204 (2) (2005) 522e531.

80.C. Unger, N. Kramer, A. Walzl, M. Scherzer, M. Hengstschlager, H. Dolznig, modeling human carcinomas: physiologically relevant 3D models to improve anti-cancer drug development, Adv. Drug Deliv. Rev. 79e80 (2014) 50e67.

81.Caruana I, Savoldo B, Hoyos V, Weber G, Liu H, Kim ES, et al. Heparanase promotes tumor infiltration and antitumor activity of CAR-redirected T lymphocytes. Nat Med (2015) 21(5):524-9. Epub 2015/04/08. doi: 10.1038/nm.3833. PubMed PMID: 25849134; PubMed Central PMCID: PMCPMC4425589.

82.Caruana I, Weber G, Ballard BC, Wood MS, Savoldo B, Dotti G. K562-Derived Whole-Cell Vaccine Enhances Antitumor Responses of CAR-Redirected Virus-Specific Cytotoxic T Lymphocytes In Vivo. Clin Cancer Res (2015) 21(13):2952-62. doi: 10.1158/1078-0432.CCR-14-2998. PubMed PMID: 25691731; PubMed Central PMCID: PMCPMC4490027.

83.Geldres C, Savoldo B, Hoyos V, Caruana I, Zhang M, Yvon E, et al. T lymphocytes redirected against the chondroitin sulfate proteoglycan-4 control the growth of multiple solid tumors both in vitro and in vivo. Clin Cancer Res (2014) 20(4):962-71. Epub 2013/12/18. doi: 10.1158/1078-0432.CCR-13-2218. PubMed PMID: 24334762; PubMed Central PMCID: PMCPMC3944408.

84.Louis CU, Savoldo B, Dotti G, Pule M, Yvon E, Myers GD, et al. Antitumor activity and long-term fate of chimeric antigen receptor-positive T cells in patients with neuroblastoma. Blood (2011) 118(23):6050-6. Epub 2011/10/11. doi: 10.1182/blood-2011-05-354449. PubMed PMID: 21984804; PubMed Central PMCID: PMCPMC3234664.

85. B. Carrion, I.A. Janson, Y.P. Kong, A.J. Putnam, A safe and efficient method to retrieve mesenchymal stem cells from three-dimensional fibrin gels, Tissue Eng. Part C Methods 20 (2014) 252e263.

86. Kunzmann V, Wilhelm M. Anti-lymphoma effect of gammadelta T cells. Leuk Lymphoma (2005) 46(5):671-80. Epub 2005/07/16. doi: 10.1080/10428190500051893. PubMed PMID: 16019504.

87. Weber G, Caruana I, Rouce RH, Barrett AJ, Gerdemann U, Leen AM, et al. Generation of tumor antigen-specific T cell lines from pediatric patients with acute lymphoblastic leukemia-implications for immunotherapy. Clin Cancer Res (2013) 19(18):5079-91. Epub 2013/07/11. doi: 10.1158/1078-0432.CCR-13-0955. PubMed PMID: 23838315; PubMed Central PMCID: PMCPMC3778051.

88. Francesca Del Bufalo , Teresa Manzo , Valentina Hoyos , Shigeki Yagyu , Ignazio Caruana , Jeffrey Jacot , Omar Benavides , Daniel Rosen , Malcolm K. Brenner . 3D modeling of human cancer: A PEG-fibrin hydrogel system to study the role of tumor microenvironment and recapitulate the in vivo effect of oncolytic adenovirus. Biomaterials 84 (2016) 76e85.

89. Guidelines for the use of cell lines in biomedical research. R J Geraghty, A CapesDavis, J M Davis, J Downward, R I Freshney, I Knezevic, R Lovell-Badge,J R W Masters, J Meredith, G N Stacey, P Thraves and M Vias. British Journal of Cancer. 2014 111, 1021–1046 | doi: 10.1038/bjc.2014.166

90. Direct presentation of non-peptide prenyl pyrophosphate antigens to human gamma delta T cells. Morita CT, Tanaka Y, Bloom BR, Brenner MB. Res Immunol. 1996 Jun;147(5):347-53

91. Low Grade Gliomas in Children. Alan Chalil and Vijay Ramaswamy. Child Neurology. J Child Neurol. 2016 Mar;31(4):517-22.

92. Diwanji TP, Engelman A, Snider JW, Mohindra P. Epidemiology, diagnosis, and optimal management of glioma in adolescents and young adults. Adolesc Health Med Ther. 2017 Sep 22;8:99-113.

93. Ming-Zhu Jin, Run-Run Han, Guan-Zhong Qiu, Xiang-Chun Ju, Ge Lou, Wei-Lin Jin. Organoids: An intermediate modeling platform in precision oncology. Cancer Letters 414(2018) 174-180.

94. Bourkoula E, Mangoni D, Ius T, Pucer A, Isola M, Musiello D, Marzinotto S, Toffoletto B, Sorrentino M, Palma A, Caponnetto F, Gregoraci G, Vindigni M, Pizzolitto S, Falconieri G, De Maglio G, Pecile V, Ruaro ME, Gri G, Parisse P, Casalis L, Scoles G, Skrap M, Beltrami CA, Beltrami AP, Cesselli D. Glioma-associated stem cells: a novel class of tumor-supporting cells able to predict prognosis of human low-grade gliomas. Stem Cells. 2014 May;32(5):1239-53. doi: 10.1002/stem.1605.

95. C. Fischbach, R. Chen, T. Matsumoto, T. Schmelzle, J.S. Brugge, P.J. Polverini,D.J. Mooney, Engineering tumors with 3D scaffolds, Nat. Methods 4 (10)(2007) 855e860.

96. Oraiopoulou ME, Tampakaki M, Tzamali E, Tamiolakis T, Makatounakis V, Vakis AF, Zacharakis G, Sakkalis V, Papamatheakis J. A 3D tumor spheroid model for the T98G Glioblastoma cell line phenotypic characterization. Tissue Cell. 2019 Aug; 59:39-43. doi: 10.1016/j.tice.2019.05.007. Epub 2019 Jun 15.

97. M.J. Bissell, D.C. Radisky, A. Rizki, V.M. Weaver, O.W. Petersen, The organizing principle: microenvironmental influences in the normal and malignant breast, Differentiation 70 (9e10) (2002) 537e546.

98. Wang TJC, Mehta MP. Low-Grade Glioma Radiotherapy Tretment an Trials. Neurosurg Clin N Am. 2019 Jan;30(1):111-118.

99. Kapałczyńska M., KolendaT., Przybyła W., Zajączkowska M., Teresiak A., Filas V., Ibbs M., Bliźniak R., Łuczewski Ł., Lamperska K. 2D and 3D cell cultures - a comparison of different types of cancer cell cultures. Arch Med Sci. 2018 Jun;14(4):910-919

100. M. Zeisberg, E.G. Neilson, Biomarkers for epithelial-mesenchymal transitions, J. Clin. Invest. 119 (6) (2009) 1429e1437.

101. K.S. Smalley, N.K. Haass, P.A. Brafford, M. Lioni, K.T. Flaherty, M. Herlyn, Multiple signaling pathways must be targeted to overcome drug resistance in cell lines derived from melanoma metastases, Mol. Cancer Ther. 5 (5) (2006) 1136e1144.

102. D. Loessner, K.S. Stok, M.P. Lutolf, D.W. Hutmacher, J.A. Clements, S.C. Rizzi, Bioengineered 3D platform to explore cell-ECM interactions and drug resis- tance of epithelial ovarian cancer cells, Biomaterials 31 (32) (2010) 8494e8506.

103. Craig Horbinski, Marina N. Nikiforova, Jill M. Hagenkord, Ronald L. Hamilton, Ian F. Pollack Interplay among BRAF, p16, p53, and MIB1 in pediatric low-grade gliomas. Neuro-Oncology, Volume 14, Issue 6, June 2012, Pages 777–789

104.Jacob K, Quang-Khuong DA, Jones DT, Witt H, Lambert S, Albrecht S, Witt O, Vezina C, Shirinian M, Faury D, Garami M, Hauser P, Klekner A, Bognar L, Farmer JP, Montes JL, Atkinson J, Hawkins C, Korshunov A, Collins VP, Pfister SM, Tabori U, Jabado N. Genetic aberrations leading to MAPK pathway activation mediate oncogene-induced senescence in sporadic pilocytic astrocytomas. Clin Cancer Res. 2011 Jul 15;17(14):4650-60.

105. Smith BD, Kasamon YL, Kowalski J, Gocke C, Murphy K, Miller CB, et al. K562/GM-CSF immunotherapy reduces tumor burden in chronic myeloid leukemia patients with residual disease on imatinib mesylate. Clin Cancer Res (2010) 16(1):338-47. Epub 2010/01/06. doi: 10.1158/1078-0432.CCR-09-2046. PubMed PMID: 20048335; PubMed Central PMCID: PMCPMC2804932.